Simulation-Based Spatially Explicit Close-Kin Mark-Recapture for Genetic Monitoring of Wildlife Populations

by

Gilia Patterson

A dissertation accepted and approved in partial fulfillment of the

requirements for the degree of

Doctor of Philosophy

in Biology

Dissertation Committee:

Andrew D. Kern, Chair

Peter L. Ralph, Advisor

Lauren Ponisio, Core Member

Rorianne Rohlfs, Core Member

Nelson Ting, Institutional Representative

University of Oregon

Fall 2025

DISSERTATION ABSTRACT

Gilia Patterson

Doctor of Philosophy in Biology

Title: Simulation-Based Spatially Explicit Close-Kin Mark-Recapture for Genetic Monitoring of Wildlife Populations

Population size is one of the most important pieces of information for monitoring conservation efforts and setting sustainable harvest limits, but it is often difficult and labor intensive to estimate. Close kin mark-recapture (CKMR) is a promising new method for estimating population size from genetic data that identifies related pairs of individuals in a sample and estimates population size from these pairs. Unlike widely used capture-recapture methods, CKMR does not rely on recapturing the same individual multiple times. This means that CKMR can be used when recaptures are difficult or impossible, such as studies involving lethal sampling, sampling at a single time point, or highly elusive species. However, a major shortcoming of current CKMR methods is that they do not model the complex spatial and social dynamics that are important in many species of conservation concern.

In my dissertation, I develop a novel spatially explicit CKMR method that models limited dispersal, spatial bias in sampling, complex social structure, and uncertainty in kin estimation. I test the method on simulations and demonstrate that it is accurate and robust to misspecified population trend. I then apply the method to elephants in Kibale National Park in Uganda and explore the feasibility of using CKMR methods to improve monitoring.

In Chapter II, I develop a novel spatially explicit CKMR method that uses a convolutional neural network trained with individual-based simulations. When tested on simulated populations, the method is able to accurately estimate population size from parent-offspring and half-sibling pairs, even when dispersal is limited and some areas of the landscape are more intensely sampled than others, a situation in which non-spatial methods are negatively biased. The method is also robust to unknown trend in population size. I apply the method to genetic data from elephant dung samples in Kibale National Park in Uganda and find that when kin pairs are assumed to be known without error, estimated population size agrees with previous estimates but with a much smaller confidence interval.

In Chapter III, I extend the CKMR method to account for two common situations in populations of conservation concern: social structure with groups of related individuals traveling together and high uncertainty in kin estimation due to a small number of sequenced loci. I then test the feasibility of using these methods for genetic population monitoring of elephants in Kibale. With 14 sequenced microsatellite loci, kin estimation is highly uncertainty and contributes to uncertainty in CKMR estimates. However, the CKMR network with recaptures still performs better than capture-recapture. With a greater number of sequenced microsatellites (56), kin estimation has very low uncertainty and the network performs very well, even when recaptures are not included.

The methods I developed in my dissertation make a valuable contribution to genetic monitoring of species with limited dispersal or complex social structure and demonstrate the power of spatially explicit simulation-based inference for conservation biology.

This dissertation includes previously unpublished coauthored material.

CURRICULUM VITAE

NAME OF AUTHOR: Gilia Patterson

GRADUATE AND UNDERGRADUATE SCHOOLS ATTENDED:

University of Oregon, Eugene, OR, USA
Oregon State University, Corvallis, OR, USA
University of Montana, Missoula, MT, USA

DEGREES AWARDED:

Doctor of Philosophy, Biology, 2025, University of Oregon
Master of Science, Statistics, 2019, Oregon State University
Bachelor of Arts, Biology and Mathematics, 2016, University of Montana

AREAS OF SPECIAL INTEREST:

Conservation genetics
Individual-based simulations
Machine learning

PROFESSIONAL EXPERIENCE:

Graduate Research Assistant, Kern-Ralph Co-Lab, University of Oregon, 2021-2025
Graduate Teaching Assistant, Department of Biology, University of Oregon, 2020-2021
Graduate Teaching Assistant, Department of Statistics, Oregon State University, 2018-2019
Research Assistant, Wheeler Lab, Department of Computer Science, University of Montana, 2016-2017
Research Assistant, Brodie Lab, Department of Biology, University of Montana, 2017
NSF REU, Santa Fe Institute, 2015

GRANTS, AWARDS AND HONORS:

The Wildlife Society Annual Meeting Best Student Oral Presentation, 2024
ARCS Foundation Oregon Scholar, 2020-2023
The Wildlife Society Biometrics Section Conference Travel Award, 2022
Justus F. Seely Award for the top first year student in Statistics, Oregon State University, 2018
Oregon State University Provost's Distinguished Graduate Fellow, 2017-2018
American Statistical Association Gertrude M. Cox Scholarship Honorable Mention, 2017
University of Montana President's Award for the Outstanding Senior in Biology – Genetics and Evolution and in Mathematics – Statistics, 2016
University of Montana Presidential Leadership Scholar, 2012-2016

PUBLICATIONS:

Patterson, G., Goodfellow, C. K., Ting, N., Kern, A. D., & Ralph, P. L. (2025). Simulation-based spatially explicit close-kin mark-recapture. *bioRxiv*, 2025-05. Submitted for publication to *Molecular Ecology Resources*.

Smith, Chris CR, Patterson, G., et al. (2024). Estimation of spatial demographic maps from polymorphism data using a neural network. *Molecular Ecology Resources*.

Carey, K. M.*, Patterson, G.*, & Wheeler, T. J. (2021). Transposable element subfamily annotation has a reproducibility problem. *Mobile DNA*, 12(1), 1-9. *Joint first authors

ACKNOWLEDGEMENTS

I am very grateful to the many people who helped me to complete my PhD.

My advisor, Peter Ralph, helped me develop a research project that fit my interests perfectly. He is an excellent and careful scientist who always made my work and writing better.

My committee gave valuable help, support, and encouragement. Andrew Kern taught me about neural networks and was always available to answer questions. Nelson Ting worked with me on elephants in Kibale National Park. I really appreciate his support in making the methods I developed useful for conservation. Lauren Ponisio and Rori Rohlfs gave excellent feedback on my research.

Claire Goodfellow allowed me to use her hard-earned elephant genetic data and encouraged me to be a conservation biologist.

The graduate students, postdocs, and scientists at UO were a wonderful community during my time in graduate school. I am especially grateful to the Kern-Ralph Co-Lab and Conservation Journal Club.

ARCS Foundation Oregon provided financial support during the first three years of my PhD.

My friends rock climbed, skied, rode bikes in the rain, swam in freezing lakes, climbed mountains, travelled, played music, and went to trivia with me. I am very glad I got to experience so much of Oregon and beyond with them.

My parents and my brother always believed in me. I am lucky to have such a supportive family and I could not have finished my PhD without them.

TABLE OF CONTENTS

Chapter Page

Chapter Page

LIST OF FIGURES

Figure Page

LIST OF TABLES

Table Page

CHAPTER I

INTRODUCTION

1.1 Overview

We are facing a human-caused extinction crisis, with many of the species on earth threatened by human activities such as habitat destruction, over harvest, introduction of invasive species, and climate change. Genetic information is a powerful tool for helping to conserve species threatened with extinction. For example, genetic data can be used to measure levels of genetic diversity in small populations, infer barriers to dispersal between fragmented subpopulations, or monitor population size. This information allows us to take actions such as introducing genetically distinct individuals, prioritizing corridors that allow maximum gene flow, or setting sustainable harvest limits [34].

All conservation genetic applications require reliable statistical methods to estimate parameters of interest. A major challenge in developing these methods is accounting for the complex spatial dynamics of the population and sampling plan. Many population genetic statistics, such as effective population size, assume either discrete populations or populations with constant density across the landscape, and estimating or interpreting these parameters in real populations with complex spatial structure is challenging [10, 60]. Methods for estimating population size from genetic data often simplify the spatial dynamics of a population. For example, these methods often assume that individuals move in circular home ranges around an activity center, an assumption that is usually violated [48].

Simulation-based inference is a promising way to account for complex spatial dynamics. Simulation-based inference methods use a simulation in place of a likelihood-based model, meaning model complexity is limited only by the ability to

simulate and not by the ability to write down and compute a likelihood [16]. Powerful population genetic simulation tools such as SLiM [29] implement spatially explicit, individual-based, population genetic simulations that can incorporate the dynamics of many species [13].

In my dissertation, I focus on a class of methods for estimating population size from genetic data called close-kin mark-recapture (CKMR). CKMR uses genetic data to identify close-kin pairs, such as parents and offspring or half-siblings, in a sample and uses these pairs to estimate population size [12, 32]. CKMR methods are very promising for improving genetic population monitoring because they do not require recaptures of the same individual. However, a limitation of current, likelihood-based methods is that they do not account for the complex spatial and social dynamics of many species. In my dissertation, I develop a spatially explicit simulation-based inference method for close-kin mark-recapture, use simulations to measure the accuracy of estimates and their robustness to misspecified population history, and apply the method to elephants in Kibale National Park in Uganda.

1.2 Background

1.2.1 Genetic population monitoring. Genetic capture-recapture is likely the most widely used method for estimating abundance of wildlife populations from genetic data. Genetic capture-recapture uses genetic samples collected non-invasively from sources such as hair or scat to identify when the same individual has been captured multiple times, then uses these recaptures to estimate population size [38]. One of the most common estimators is based on the multinomial distribution and is implemented in the R package `capwire`[41, 44]. This estimator models sampling individuals like drawing balls from an urn with replacement. If each individual is equally likely to be sampled, then individual capture counts follow a multinomial

distribution with probabilities $1/N$, where N is population size. In most populations, some individuals are more likely to be captured than others. The `capwire` package models this situation by assuming that individuals in the population can be divided into two distinct classes with two different capture probabilities [41, 44].

Close-kin mark-recapture is conceptually similar to capture-recapture, but instead of recapturing individuals, it recaptures genotypes through close-kin pairs. The probability of capturing a close-kin pair depends on fecundity and survival in addition to population size. The basic likelihood models for parent-offspring and half-sibling pairs are described in Bravington, Skaug and Anderson [12]. For mother-offspring pairs where female fecundity after reproductive maturity does not vary with age, the ages of sampled individuals are known, and sampling is lethal, the probability that individual i is the mother of individual j is the expected reproductive output of i at the time j was born over the total expected reproductive output of all females alive when j was born. Since all mature females are assumed to be equally likely to be j's mother, the probability of a mother-offspring kin pair is

$$\mathbb{P}(K_{ij} = MO|z_i, z_j) = \frac{\mathbb{E}[R_i(y_j)|y_i, t_i]}{\mathbb{E}[R_+(y_j)]} = \frac{\mathbb{I}[y_i + \alpha \leq y_j < t_i]}{N_{Fy_j}}$$

where (y_i, y_j) is year of birth of each pair, $R_i(y_j)$ is the reproductive output of i in the year j was born, $R_+(y_j)$ is the total reproductive output of all females in the year j was born, $\mathbf{z_i} = (t_i, a_i)$ is the year of sampling and the age at sampling of each individual, α is the age at which females are reproductively mature, and N_{Fy_j} is the number of mature females in the year individual j was born. To estimate N_{Fy_j}, the relationships of each sampled pair of individuals are assumed to be independent, and so the likelihoods of each pair are multiplied to get a pseudo-likelihood. This pseudo-likelihood is then maximized to get an estimate of N_{Fy_j}. Pseudo-likelihoods for half-siblings are calculated similarly.

CKMR methods can be significantly biased when factors that affect probabilities of observing kin pairs are not accounted for, and a major factor is space. When related individuals tend to be close together due to limited dispersal and sampling is spatially biased, more kin pairs are sampled than expected under random sampling and so non-spatial estimates of population size are negatively biased [15]. However, incorporating complex spatial dynamics into likelihood-based models is challenging. The one existing spatially explicit method, Sévêque et al. [51], introduces many assumptions to simplify the likelihoods, including assuming that relative population density across the landscape is known and that dispersal is independent between individuals.

1.2.2 Simulation-based inference. In simulation-based inference, a simulation takes the place of a statistical model. The simulation takes as input the parameters we are interested in estimating, $\boldsymbol{\theta}$, and outputs data, $\boldsymbol{x}$. The simulation can be any type of stochastic simulation. It could be very simple, such as drawing values from two different distributions, or complex, such as the individual-based models used in my dissertation. One of the simplest methods for simulation-based inference is Approximate Bayesian Computation (ABC). ABC determines a prior distribution for $\boldsymbol{\theta}$, draws many values of $\boldsymbol{\theta}$ from the prior distribution, simulates data for the drawn values of $\boldsymbol{\theta}$, then compares the simulated data to observed data. In the simplest implementation of ABC, if the simulated data are close to the observed data, the value of $\boldsymbol{\theta}$ is accepted and all of the accepted values form a posterior distribution for $\boldsymbol{\theta}$.

ABC has been used widely in population genetics and evolutionary biology since at least the 2000s [6]. In the past 10 years, simulation-based inference methods using machine learning have become more broadly used [16]. For example, instead of using

ABC to get a posterior estimate for $\boldsymbol{\theta}$, `sbi` [57] trains a neural network to predict the parameters of the posterior distribution from observed data.

Another machine learning method for simulation-based inference is based on convolutional neural networks (CNNs), a type of network designed for analyzing images. In these methods, the observed data are one or more images, and the CNN is trained on simulations to predict the parameters of interest. CNNs are especially useful for spatial data, because unlike other methods such as ABC, CNNs do not require converting maps to a set of summary statistics and so can take advantage of all spatial information available in the observed data. CNNs have been successfully used for estimating spatial population genetic parameters, including density and dispersal [52, 53].

1.2.3 Elephants in Kibale. African elephants in Uganda have faced intense threats over the past few generations from habitat loss, poaching, and human conflict. These threats were most intense during the reign of Idi Amin in the 1970s, and many populations were thought to be on the brink of extinction [39, 42]. Elephant populations have since significantly increased; however, we still know very little about many of these populations.

Kibale National Park is located in the Albertine Rift in southwestern Uganda and protects a population of African elephants that are primarily hybrids of the two species of African elephants, savanna (*Loxodonta africana*) and forest (*Loxodonta cyclotis*) [25]. Because Kibale is primarily forested, monitoring elephants in the park is challenging and labor intensive, and we know very little about the population. Two recent population size estimates suggest that the population has recovered since the 1970s. In 2021, Daniel, Edward and Kennedy [17] performed a cut-transect survey of elephant dung and estimated that population size was 566 with a 95% confidence

interval of 377 to 850. In 2025, Goodfellow et al. [25] performed a capture-recapture analysis based on genetic data from elephant dung and estimated that population size was 573 with a 95% confidence interval of 410 to 916.

Elephant monitoring in Kibale could potentially benefit from adding close-kin mark-recapture methods. The samples collected by Goodfellow et al. [25] for genetic capture-recapture contain many kin pairs [26], and so using the information contained in these kin pairs could reduce uncertainty in estimates of population size. However, implementing CKMR methods for the elephants in Kibale is challenging because of their complex social structure and the low-quality genetic data collected from dung. Elephants have a matrilineal society and related females travel together in social groups [3], so dung samples from the same area tend to have many kin pairs. Goodfellow et al. [25] were only able to sequence 14 microsatellites from dung samples, leading to high uncertainty in identifying kin pairs.

1.3 Outline of dissertation

In my dissertation, I develop simulation-based spatially explicit close-kin mark-recapture methods to account for limited dispersal, spatial bias in sampling, complex social structure, and low-quality genetic data, and to take advantage of additional information about population size available from the spatial pattern of kin pairs on the landscape. I then apply these methods to elephants in Kibale National Park in Uganda and determine the feasibility of using kin-based methods for future genetic monitoring.

Chapter II: Simulation-based spatially explicit close-kin mark-recapture. In Chapter II, I develop and test a simulation-based spatially explicit close-kin mark-recapture method using a convolutional neural network. The network takes as input images representing maps of sampling intensity, kin pairs, and, if

available, recaptures, and outputs a population size. The network is trained on spatially explicit, individual-based simulations.

I first test the method on simulated populations with high spatial structure due to limited dispersal. When both the test simulations and training simulations have constant population size over time, the method is highly accurate and estimates population size to within 6% of the true value, even with high spatial bias in sampling. When population trend is misspecified and the test simulations are decreasing or increasing in size, the method is much less accurate. However, training the network on a range of population trends increases its robustness, and it is able to estimate population size to within 10% of the true value even when the population is increasing or decreasing in size.

I next demonstrate the method on the elephants of Kibale National Park using the dataset collected by Goodfellow et al. [25]. When I assume that parent-offspring pairs are known without error, the network estimates population size within Kibale to be 450 with a 95% confidence interval of 323 to 620. This estimate is consistent with the previous two estimates of population size in the park, but with a 32% smaller confidence interval.

In Chapter II, I show that CKMR methods have the potential to greatly improve population size estimates in Kibale. However, many of the assumptions made in the analysis are unrealistic for the Kibale elephants. I assumed that we know parent-offspring pairs without error, but with only 14 microsatellites, there is high uncertainty in these kin pair estimates, and so the analysis probably greatly underestimates uncertainty in population size. I assumed that elephants move independently of each other, but elephants have a matrilineal social structure and

parent-offspring pairs are often moving together in the same social group, a pattern that may bias estimates of population size if not accounted for.

Chapter III: Estimating population size in African elephants with simulation-based spatially explicit close-kin mark-recapture. In Chapter III, I extend the methods from Chapter II to account for uncertainty in kin pair identification and social structure, two factors that are important for elephants in Kibale and for other populations of conservation concern. I then test the feasibility of using these methods for monitoring elephants in Kibale.

To train and test the network, I develop a genetic individual-based simulation model of elephants. The simulation includes matrilineal social structure and inheritance of the same microsatellite loci sequenced from dung in Kibale. I parameterize the model using prior studies on forest and savanna elephants and show that the model accurately represents fertility, reproductive value, and group size of elephants.

To explore uncertainty in kin estimation, I implement a likelihood-based approach for estimating kin and measure the expected error in estimating parent-offspring and half- and full-sibling pairs. I test both the 14 microsatellites sequenced for Kibale and a hypothetical dataset with 56 microsatellites derived by copying the frequencies of the 14 microsatellites. With 14 microsatellites, kin estimation has fairly high error. For 56 microsatellites, kin estimation is very reliable and correctly identifies over 95% of parent-offspring pairs.

To account for uncertainty in kin estimation in the network, I add a kin estimation step to the simulation pipeline and train the network from Chapter II to estimate population size from the estimated parent-offspring and half-and full-sibling pairs and sampling intensity, and for one network, recaptures. With 14 microsatellites,

estimated population size has very high error when not using recaptures, with a mean relative absolute error of over 0.5. Adding recaptures greatly decreases error and leads to better estimates than capture-recapture, with mean relative absolute error of 0.36 for the network and 0.413 for capture-recapture. With 56 microsatellites, estimated population size has very lower error. Estimates have a mean relative absolute error of 0.27 when not using recaptures and 0.25 when using recaptures.

Obtaining samples of elephant dung from Kibale is time and labor intensive. In Chapter III I demonstrate that CKMR is a feasible way to reduce the number of samples needed for population monitoring.

1.4 Summary

In my dissertation, I develop a spatially explicit close-kin mark-recapture method, test the method on simulated data, and apply the method to elephants in Kibale National Park. This dissertation is a thorough exploration of the use of simulation-based spatially explicit CKMR for genetic monitoring of elephants and other wildlife species with social structure and small numbers of sequenced loci.

Both Chapter II and Chapter III are coauthored and will be published. Chapter II is coauthored with Claire Goodfellow, Nelson Ting, Andrew Kern and Peter Ralph and has been submitted to *Molecular Ecology Resources*. Chapter III is coauthored with Silas Tittes, Nelson Ting, and Peter Ralph and will be submitted for publication in the future.

CHAPTER II

SIMULATION-BASED SPATIALLY EXPLICIT CLOSE-KIN MARK-RECAPTURE

This chapter is coauthored with Claire Goodfellow, Nelson Ting, Andrew Kern and Peter Ralph. Claire Goodfellow estimated kin pairs for the analysis. Claire Goodfellow and Nelson Ting provided input on the elephant model. Peter Ralph and Andrew Kern contributed to the manuscript. I implemented all analyses except kin estimation and wrote most of the manuscript.

2.1 Introduction

Population size is one of the most important pieces of information that informs the conservation and management of wildlife populations, but it is often challenging and expensive to estimate. One of the most promising sources of information about population size is genetic data. Genetic material can be relatively easily collected from sources such as hair, scat, or hunter harvests, and it is increasingly affordable to generate genotype information from this material. Thus developing accurate statistical methods to use genetic data has the potential to improve monitoring and conservation efforts for many species.

One of the most commonly used methods for estimating population size from genetic data is genetic capture-recapture, which uses genotype information sampled non-invasively, for example, from hair or scat, to identify when the same individual has been captured multiple times and then estimates census population size from these recaptures [38, 41]. Genetic capture-recapture models can account for many of the complexities of real populations, such as unequal capture probabilities due to behavioral responses to trapping or differences in the amount of DNA shed by individuals [38]. More recently, these models have been extended to use spatial

information. Spatially explicit capture-recapture models can account for the spatial distribution of sampling locations on the landscape, ecological variables that impact the movement of individuals, and variation in population density across the landscape [20, 21]. Genetic capture-recapture and spatially explicit genetic capture-recapture have been used to effectively monitor many species including grizzly bears from hair snares [9], red deer from scat [19], and fishers and grey foxes from hair traps [27].

Close-kin mark-recapture (CKMR) is a promising, recently developed type of method that uses genetic data to identify pairs of close kin among a set of sampled individuals, and then uses these pairs in a way conceptually similar to recaptures to estimate abundance [12, 32]. Because CKMR does not require recaptures, it has the potential to improve monitoring for many of the species for which genetic capture-recapture models cannot be used or do not provide good estimates. These include systems that require lethal sampling and systems with elusive, hard to capture individuals. CKMR models have been used to estimate abundance in several species, including southern bluefin tuna [11], white sharks [30], thornback rays [58], brook trout [49], speartooth sharks [43], flying foxes [37], caribou [40], bearded seals [56], and lemon sharks [55]. However, a major limitation to using CKMR methods more broadly is that spatially explicit methods that account for population structure and spatial biases in sampling are limited, with only one recently published method available [51]. When dispersal is limited (i.e., when spatial population structure exists), kin pairs are expected to be found more closely together, and so when the landscape is sampled more intensely in some areas than others, the number of sampled kin pairs is larger than expected. This results in downwardly-biased estimates of population size when non-spatial methods are applied [15].

Current CKMR methods (with the exception of Conn [14]) are generally based on an analytic likelihood of observing a given kin relationship for each pair of individuals in the sample. The basic likelihood models for parent-offspring and half-sibling pairs are described in Bravington, Skaug and Anderson [12]. Most applications of CKMR incorporate more complicated population dynamics into these likelihood models by necessity. For example, Lloyd-Jones et al. [37] added a parameter for recent population size trend to estimate both the trajectory of the population and abundance in flying foxes. Swenson et al. [55] developed models that incorporated uncertainty in aging, fluctuations in population size, and intermittent breeding. Finally, Sévêque et al. [51] accounted for spatial population structure when relative density across the landscape is known and dispersal is independent between individuals.

Adding spatial information to likelihood methods becomes much more difficult when models of movement and dispersal are complex, both because formulating an appropriate likelihood becomes challenging and because computing the likelihood becomes computationally intensive. Simulation-based inference provides a promising way of overcoming these challenges. Simulation-based methods do not require a likelihood and the complexity of the model is limited only by the ability to simulate reasonable approximations to the true population dynamics [16]. Recently, simulation-based inference models have begun to be applied to non-spatial close-kin mark-recapture and show great promise. Conn [14] implemented individual-based simulations and used observed counts of kin pairs grouped by age classes with Approximate Bayesian Computation (ABC) to infer posterior distributions of abundance and survival. This approach accounted for non-independence of pairs of individuals and dealt with the inability to distinguish half-sibling relationships from

aunt-niece or grandparent-grandchild, two difficulties with previous likelihood-based methods.

In this paper, we develop a novel simulation-based spatially explicit close-kin mark-recapture method, named CKMRnn. We create synthetic "images" of kin pairs and sampling intensity across the landscape that compactly encode the spatial information available for the system, then train a deep convolutional neural network (CNN) on simulated images to estimate population size. Similar simulation-based methods utilizing CNNs have been demonstrated to be effective at inferring population genetic parameters from genetic data [23], and more specifically, for spatial population genetic parameters such as density and dispersal [52, 53, 54].

We first test CKMRnn on simulated populations with limited dispersal, spatially biased sampling, and varying trends in population size and demonstrate that our method is both accurate and robust. We then apply CKMRnn to estimate the population size of African elephants (*Loxodonta africana* and *L. cyclotis*) in Kibale National Park in Uganda using data from dung samples collected by Goodfellow et al. [25]. Like many populations of conservation concern, the Kibale elephant population is challenging to monitor and has strong spatial patterns in kin pairs across the landscape that could lead to bias when using traditional, non-spatial CKMR methods. This makes Kibale elephants a good system to test the feasibility of our method. We find that CKMRnn agrees with traditional capture-recapture point estimates of elephant population size, but provides a 32% smaller confidence interval.

2.2 Methods

2.2.1 CKMRnn workflow. The first step of the CKMRnn workflow is to process the empirical data to create a collection of images summarizing the observed kin pairs and sampling effort. The images are all of the same dimension

and show the geographic region of interest. One image summarizes the intensity of the sampling effort across the region as a heatmap and the other images show the observed kin pairs and/or recaptures by connecting their sampling locations with line segments (see Figure A.2). The precise details and number of these images may differ depending on the system. For instance, "sampling effort" could be measured as the amount of time spent searching in each section of a study landscape, as the number of samples found in each section, or as a variety of other metrics. The total number of images will depend on how many types of close kin and/or recaptures are used. For instance, one could apply the method to *only* mark–recapture data, with only one image connecting the mark/recapture locations; while another situation might have separate images for full siblings, half siblings, parent-offspring pairs, etcetera. In our application to elephants, we made these images by first projecting the GPS coordinates of each sample onto a rectangular surface using GIS tools in R, then creating images using the Python Image Library.

The second step is to develop a spatially explicit individual-based simulation of the system in question, including the empirical sampling scheme. In our examples we developed simulations using the population genetic simulation software SLiM [29], building on the spatial simulation methods described in [13]. The dynamics of the simulation are based on previous knowledge of the population of interest. The simulation does not need to perfectly match the empirical population, and we can account for uncertainty in some of the parameters of the simulation by choosing a reasonable range of values, similar to a prior distribution, and then simulating across this range.

The third step is to generate training data and train the neural network. Training data are produced by running many simulations with a range of population sizes (and

possibly other parameter values), then processing each simulated sample to produce images of the same dimensions and summarizing the same information as the images created for the empirical data. The convolutional neural network (CNN) is then trained on this training data to estimate population size from images.

The final step is to estimate population size and uncertainty for the empirical population. The point estimate of population size is obtained by passing the images derived from the empirical data to the trained network. Then, a distribution of parametric bootstrap replicates is generated by running many simulations with population size set to the point estimate and passing the resulting images for each simulation through the trained network. A confidence interval is then computed from this distribution of estimates.

We describe these steps in more detail in our examples below. The code for the CKMRnn workflow is available in the CKMRnn GitHub repository (`https://github.com/giliapatterson/CKMRnn`).

2.2.2 Simulation tests. We start by evaluating the performance of CKMRnn using simulations. Our simulations closely follow those used by Conn et al. [15], who used simulations modeled on bearded seals to demonstrate that non-spatial CKMR can be biased in the presence of spatial structure. We implemented the simulation using the simulation software SLiM [29], incorporating age-dependent survival and reproduction, limited dispersal, and lethal sampling. The simulation is stochastic and individual based and takes place in continuous space.

The simulation proceeds on a homogeneous 10×10 square landscape (the units are arbitrary, but taking density estimates from Fuirst et al. [24], one unit might roughly correspond to 10km). The population is initialized with N_0 individuals, with an even sex ratio, where initial individual locations are chosen uniformly across the

landscape. N_0 is varied between simulations to obtain different population densities. The initial ages for individuals are assigned from the stable age distribution based on a non-spatial Leslie matrix model with the same survival and reproduction parameters as our simulation. Each timestep of the simulation represents one year, and proceeds through reproduction, survival, and dispersal. We simulated 40 years of burn-in, then recorded and sampled from all individuals that died in years 40 through 60.

In each time step, first, fertile females mate and reproduce. A female of age a is fertile with probability $1/\left(1+\mathrm{e}^{-1.264(a-5.424)}\right)$. If a female is fertile, she chooses a mate from all males within a radius of $1/\sqrt{\pi}$. Older males are more likely to be chosen: the probability that a male of age a_m within the circle is chosen as a mate is proportional to $1/(1+\mathrm{e}^{-1.868(a_m-6.5)})$. Numerical constants in these expressions were taken from Conn et al. [15]. If at least one male is within the circle, the female produces one offspring, and the offspring's location is set to that of the female's.

Next, each individual of age a dies with probability

$$S_a = \exp\left[-C\left((\eta_1 a)^{\eta_2} + (\eta_1 a)^{1/\eta_2} + \eta_3 - (\eta_1(a-1))^{\eta_2} - (\eta_1(a-1))^{1/\eta_2}\right)\right]$$

where $C = 1.111$, $\eta_1 = \exp(-2.904)$, $\eta_2 = 1+\exp(0.586)$, and $\eta_3 = \exp(-2.579)$. The parameters η_1, η_2, and η_3 were again taken from Conn et al. [15]. The parameter C was calculated using the Leslie matrix model and chosen so that the population size stays constant. We also introduced a linear population trend into the simulation by multiplying survival probabilities by 1.01 or 0.99.

Finally, each individual moves to a new location chosen from a bivariate Normal distribution centered on the original location with standard deviation $\sigma = 1$. This means that all individuals move on average a distance of 1 unit, or roughly 10 km, each year.

To simulate sampling, we divided the landscape into a grid of one hundred 1×1 squares, assigned a sampling intensity $I_{i,j}$ to each grid cell, and then took a random sample of $\lceil n \cdot I_{i,j} / \sum_{i=1}^{10} \sum_{j=1}^{10} I_{i,j} \rceil$ individuals from the i, j^{th} grid cell, for each cell, where n is the total sample size. In all sampling plans, sampling intensity was constant across rows and increased linearly in columns, so that $I_{i,j} = 1 + \alpha(i-1)/10$ for some α. We implemented three sampling plans: (1) uniform, where all intensities were equal ($\alpha = 0$); (2) medium spatial bias, where the bottom row of the landscape was 15 times more likely to be sampled than the top row ($\alpha = 15$); and (3) high spatial bias, where the bottom row of the landscape was 30 times more likely to be sampled ($\alpha = 30$).

We generated two sets of simulated data, one with constant population size and one with varying population trends. For the constant size dataset, we ran 2601 simulations with initial population sizes between 5000 and 20000. For the varying trends dataset, we ran 2601 simulations with each of the three trends (constant, increasing, and decreasing). We recorded final and average population sizes for each simulation. For each simulation, we sampled $n = 2000$ individuals using uniform, medium-bias, and high-bias sampling plans. The constant size dataset had 7803 total simulated samples and the varying trends dataset had 23409 total samples. For each sample, we created three 500×500 pixel images. The first is a map showing relative sampling intensity across the landscape (the 10×10 image of $I_{i,j}$). The second two show half-sibling and parent-offspring pairs, respectively, with pairs connected by line segments.

The neural network architecture is summarized in Figure A.2. The first layer is a convolutional layer with 3 input channels, one for each 500×500 image, and 32 output channels. This layer has a kernel size of 6 and padding of 3. It performs a

2d convolution separately on each input channel (image) and then sums the result. Each of the 32 output channels is a 500×500 matrix that is the result of a separate convolution. Each matrix is passed through a ReLU layer that converts negative entries to 0 and then through a max pooling layer with a kernel size of 2. The max pooling layer divides each of the 32 500×500 matrices into 250 2×2 squares and keeps only the maximum value in each square, resulting in 32 250×250 matrices. The next three layers are another set of convolution, ReLU, and max pool layers. This time, the convolution layer has 32 input channels and 64 output channels and so the output of these 3 layers is 64 125×125 matrices. These matrices are flattened into a single, 1×10^6 vector and then passed through a fully connected layer with 1024 output nodes. The resulting 1×1024 vector is then passed through a ReLU layer and a dropout layer. The dropout layer sets 0.2 of the elements of the vector to 0. The final layer is a fully connected layer that outputs a single number, the estimated population size.

We trained two neural networks, one on the constant size dataset and one on the varying trends dataset. For each network, one half of the simulations were used for training, one quarter for validation, and one quarter for testing. We trained the network to minimize mean-squared error loss using the Adam optimizer and batches of size 64. Training was run for 20 epochs.

2.2.3 Estimation of population size in African elephants. We next used CKMRnn to estimate population size of African elephants in Kibale National Park in Uganda using the genetic samples collected by Goodfellow et al. [25]. The dataset contains 256 samples collected from dung piles across Kibale (Figure 1A). These samples were collected on 49 days between November 2020 and August 2021 from locations around the park where elephants were known to spend time. The

samples were genotyped at 14 microsatellite loci and these genotypes were analyzed with `GenAlEx v. 6.51b2` and `MLRelate` [33] to identify unique individuals and parent-offspring pairs [25, 26].

We first processed the empirical data to create three grayscale images for input to the neural network, one for sample locations, one for parent-offspring pairs, and one for recaptures, as shown in Figure 1. The dimensions of each image were 566×837 pixels, and Kibale National park is approximately 38×56 km, so this corresponds to 15 pixels per kilometer. To create the images, we pooled all data together ignoring date of collection.

For sampling, we divided the outline of Kibale into a grid of 1 km by 1 km cells, with 771 cells total, and determined the number of samples in each cell. Samples taken from just outside the boundary of the park were assigned to the closest grid cell. The shade of each cell of the sampling image was then proportional to the number of samples, with cells with the maximum number of samples set to white and cells with no samples set to black. Because we do not have information on locations that the field team visited but did not find elephant dung, this image does not represent sampling intensity in the same way as in the simulation tests. It instead encodes information about spatial bias in sampling through the locations of samples.

For recaptures and parent offspring pairs, we first filtered the dataset to retain only the first location for any instances where the same individual was sampled multiple times on the same day. For recaptures, we connected the location of the two captures with a line segment. When an individual was captured more than twice, we sorted the recaptures by time and connected only subsequent pairs: first recapture to second recapture, second to third, and so on.

For parent-offspring pairs, we connected the location of the parent when it was sampled to the location of the offspring when it was sampled. Some of the individuals in parent-offspring pairs were sampled multiple times. For plotting these pairs, we treated each of the samples like a unique individual, and so these pairs are represented by multiple line segments.

To generate training data for the neural network, we developed an individual-based, continuous space SLiM simulation modeled on the elephant population within Kibale National Park. The dynamics and demographic parameters of the simulation model were based on previously published work on forest and savanna elephants [2, 3].

The simulation is set within the boundaries of Kibale National Park and simulated elephants cannot disperse or move beyond the boundary. Each elephant has a location within the park and can move around from year-to-year and day-to-day. Reproduction and survival happen once each year. Mortality is primarily age-based, with elephants living a maximum of 55 years. We varied three parameters of the simulation when generating our training set: population size (N), which was drawn from a uniform distribution between 100 and 1500; yearly movement distance (σ_D), drawn from a uniform distribution between 5 km and 10 km; and the radius within which a female chooses a mate (σ_M), also drawn from a uniform distribution between 5 km and 10 km.

The population is initialized with $1.25N$ elephants, half female and half male, with locations chosen uniformly within the boundaries and ages chosen uniformly from 0 to 60. We keep track of the last year a female reproduced, and the "years since last reproduction" for elephants in the initial population were chosen uniformly between 0 and 6.

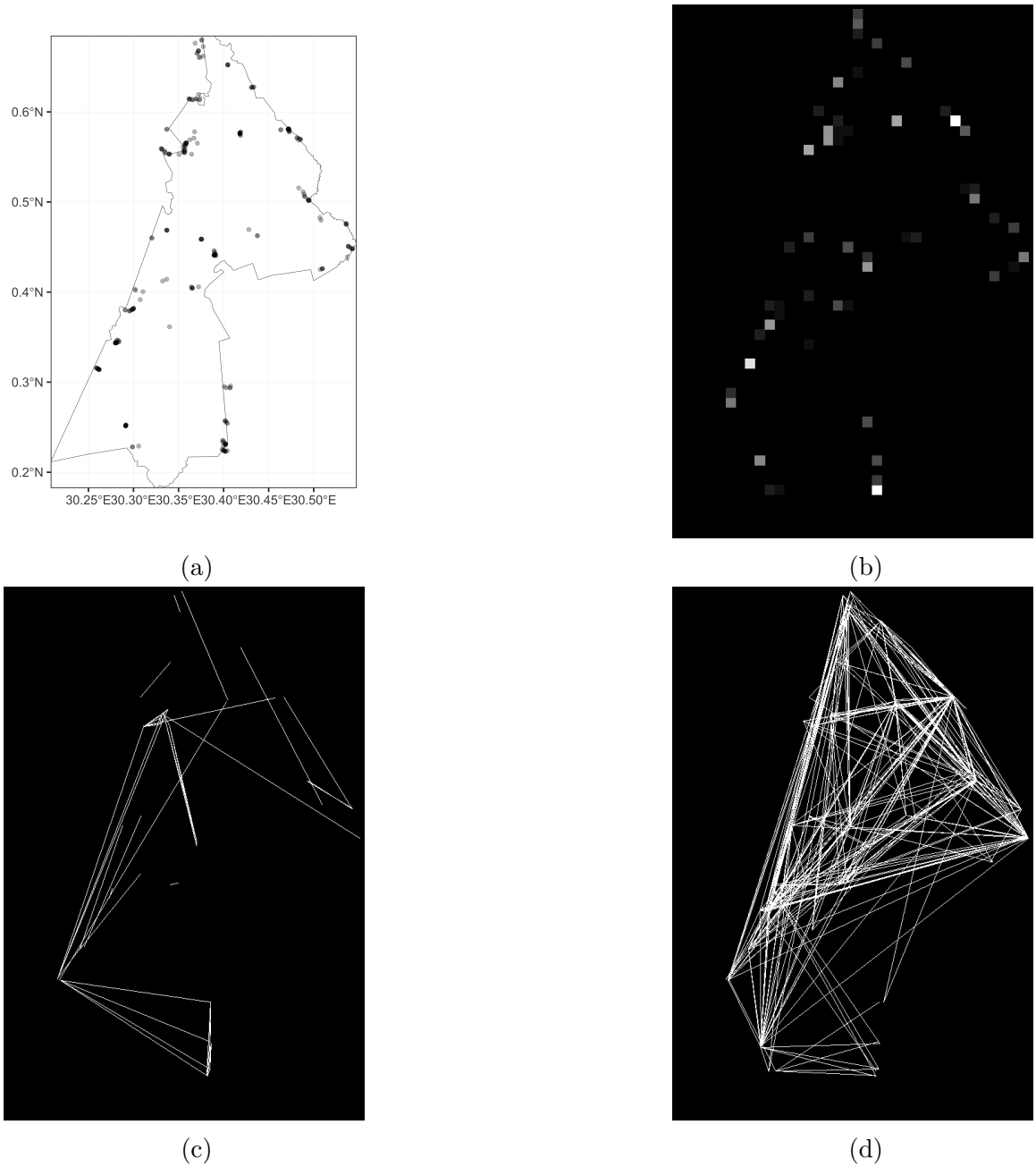

Figure 1. Empirical data for African elephants in Kibale National Park. **(a)** Locations of samples (points) within the park (outline). **(b-d)** Images provided to the neural network, showing **(b)** sampling intensity (pixel lightness is proportional to number of samples in that 1km $\times$ 1km pixel); **(c)** recaptures (lines connect original and recapture locations); and **(d)** parent-offspring pairs (lines connect parent and offspring sampling locations).

Each time step of the simulation represents one year, and proceeds through reproduction, survival, and dispersal steps. In the reproduction step, the probability each female is fertile and therefore can reproduce if a mate is available is determined by her age and the number of years since she last reproduced. A female of age a and with $y > 2$ years since last reproduction is fertile with probability

$$\min\left[\left(1+\exp(-0.5(a-20))\right)^{-1}\left(1+\exp(-2(y-5))\right)^{-1},1\right].$$

For females with two or fewer years since last reproduction, the probability is 0. For females with at least 6 years since last reproduction, fertility probability starts at 0 and then increases to 1 between ages 10 and 30. For females with 3-5 years since last reproduction, this curve is shifted downward and plateaus at 0.02, 0.12, and 0.5, respectively (Figure A.1). Each fertile female chooses a mate uniformly randomly from all males of age greater than 25 that are within a radius σ_M of the female. When a female mates she produces one offspring. To represent the long gestation times of elephants, the offspring is added to a separate population of fetuses, where it remains for two years. If the mother of a fetus is alive after two years, the fetus is transferred to the main population, its age is set to 0, and its location is set to the location of its mother.

Survival is a combination of age-dependent and density-dependent mortality. We took five year probabilities of survival from Armbruster and Lande [2] and converted to one year survival probabilities by taking the fifth root (Table 1). In each time step, we multiplied these fixed survival probabilities for each age by N divided by the current population size, ensuring that the population size stays relatively constant around the parameter N.

In the dispersal step, all individuals move around within the bounds of Kibale. New locations for each individual are chosen by sampling a potential new location

Age	Female	Male
0-4	0.871	0.871
5-9	0.976	0.976
10-14	0.976	0.976
15-19	0.979	0.979
20-24	0.980	0.984
25-29	0.975	0.930
30-34	0.975	0.924
35-39	0.974	0.930
40-44	0.970	0.909
45-49	0.910	0.652
50-54	0.833	0.803
≥ 55	0.000	0.000

Table 1. One year survival probabilities for simulated elephants. Probabilities were calculated by taking the fifth root of five year survival probabilities from Armbruster and Lande [2].

from a bivariate normal distribution with standard deviation σ_D centered on the current location, checking if the potential new location is within Kibale, and if not, choosing a new potential location. This process is repeated until a location within Kibale is found or until twenty potential locations are drawn, whichever comes first. If no new location is found, the elephant stays in its original location.

Sampling takes place in year 201 after a burn-in period of 200 years. Unlike in other years, when net movement across the year was simulated in a single step, during the dispersal step of the sampling year, 365 days of movement are simulated. Each day, the new locations of individuals are chosen using the same process as for yearly dispersal, but with standard deviation $\sigma_D/\sqrt{365}$. This means that 365 daily movement steps are equivalent to one year of dispersal (except for boundary effects).

To sample our simulated populations, we closely replicated the empirical sampling plan. We first converted the locations and times of empirical samples into SLiM locations and days. For sampling locations, we found the centers of the 1 km

by 1 km grid cells that were closest to the locations of the empirical elephant samples, and then used the unique centers as potential sampling locations. For days, we set the first date of sampling to SLiM day 1, and then converted subsequent dates of sampling to SLiM days by calculating the number of days since the first date of sampling. This process led to 53 sampling locations and 49 sampling days. We set the sample size to $n = 256$, matching the empirical sample size.

For each sampling day, a potential sampling location is chosen from the list of empirical locations at random, all individuals within a radius of 1 km from the location are sampled, and then a new potential sampling location is chosen. This process is repeated until either the total number of individuals sampled in the simulation reaches n or the number of individuals sampled that day reaches $n/49$. We recorded recaptures, parent-offspring pairs, and locations for sampled simulated individuals.

We ran 10,000 replicate simulations with population sizes drawn uniformly randomly between 100 and 1500 and values of σ_D and σ_M drawn independently from uniform distributions on [5 km, 10 km]. For each simulated sample, we plotted grayscale images of sampling intensity, recaptures, and parent offspring pairs using the same procedure as for the empirical data.

The elephant neural network has a nearly identical architecture to the network in the simulation tests described above. The only difference is that the input size of each of the three images is 566×837 instead of 500×500 and so the input for the first fully connected layer is a 1×1908480 vector instead of a 1×10^6 vector. We trained the elephant network using 7500 simulations and reserved the remaining 1500 for testing. We trained the network to minimize mean-squared error loss using the Adam optimizer and batches of size 10. Training was run for 20 epochs. We implemented the network in the Pytorch package.

2.3 Results

2.3.1 Simulation tests. To evaluate the performance of CKMRnn on simulated populations, we used the two sets of bearded seal simulations (constant trend and varying trend) to create three tests. First, we measured the performance of CKMRnn in situations where the dynamics of the true population exactly match the training data by training CKMRnn on half of the constant-size set and testing on part of the other half. Second, we measured performance when population trend is misspecified (i.e., there is a trend in the real system not reflected in the simulations) by training on the constant-size set and testing on the varying trend set. Finally, we measured performance when population trend is unknown but not misspecified by training on half of the varying trend set and testing on part of the other half. The last test reflects a general strategy for dealing with unknown aspects of the empirical system: simulate across a "prior" range of situations, so that the network is trained to be robust to variation induced by the unknown aspects.

2.3.1.1 Accuracy with biased sampling. When CKMRnn was both trained and tested on constant-size simulations, the predicted population sizes closely matched true population sizes for all levels of sampling bias (Figure 2a). On average, CKMRnn estimated population sizes within 6.3% of the true population size across all levels of spatial sampling bias. Estimates were unbiased, with mean relative error less that 1.5% in all cases: 0.011, 0.001, and 0.013 for uniform, medium bias, and high bias sampling plans, respectively (Figure 2b, Table 2).

As true population size increased, estimates appeared to become less accurate and more negatively biased, so we also divided the test set into populations below and above size 12000 and computed relative error for each. Mean relative error (MRE) and mean relative absolute error (MRAE) were about the same for $N < 12000$ and

CKMRnn performance with sampling bias						
Spatial sampling bias	Mean relative absolute error (MRAE)	MRAE $N <$ 12000	MRAE $N \geq$ 12000	Mean relative error (MRE)	MRE $N <$ 12000	MRE $N \geq$ 12000
uniform	0.063	0.064	0.060	0.011	0.034	-0.039
medium	0.051	0.052	0.049	0.001	0.014	-0.024
high	0.050	0.053	0.046	0.013	0.025	-0.011

Table 2. CKMRnn performance with varying levels of spatial sampling bias, as depicted in Figure 2a. Here, the population sizes of both the tested simulations and the simulations used to train the model were constant in time (i.e., no population trend). Relative absolute error is calculated as $|\text{predicted} - \text{true}| / \text{true}$ and relative error as $(\text{predicted} - \text{true}) / \text{true}$. Separate results are shown for simulations with true N above and below 12,000.

$N \geq 12000$ but errors were shifted slightly upward for $N < 12000$ and downward for $N \geq 12000$. This shift was especially apparent for uniform sampling, with MRE for $N < 12000$ of 0.034 and MRE for $N \geq 12000$ of -0.039. However, errors were still centered near zero. For our simulations we expect estimates to become more negatively biased as population size increases because we are sampling a smaller proportion of the population and will get fewer parent-offspring and half-sibling pairs. Because dispersal is limited, sampling plans with spatial bias tend to sample more related pairs for the same sample size and so this pattern will be less prevalent for biased plans.

2.3.1.2 The effect of misspecified population trend. When CKMRnn was trained on constant size simulations and tested on simulations with increasing or decreasing trend, estimates of current population size were less accurate and more biased (Figure 3). Overall, CKMRnn estimated final population size to within about 20% of the true value for all sampling plans (Table 3). The estimates were positively biased for test simulations with decreasing population size and negatively biased

CKMRnn performance for misspecified population trend			
Population trend	Spatial sampling bias	Mean relative absolute error	Mean relative error
decreasing	uniform	0.206	0.206
increasing	uniform	0.234	-0.232
decreasing	medium	0.224	0.224
increasing	medium	0.211	-0.211
decreasing	high	0.208	0.207
increasing	high	0.192	-0.192

Table 3. CKMRnn performance on data with misspecified population trend. The method is trained with simulations of constant population size, but tested on simulations with population size increasing or decreasing by 1% per year.

for those with increasing size (Figure 3). This is expected: when population size is decreasing, the number of kin pairs is smaller than expected for a constant size population and so if the trend is not accounted for, estimates will be negatively biased, and vice versa for increasing trend.

2.3.1.3 Training for robustness to population trend. Finally, we tested our ability to make CKMRnn robust to unknown population trend by training the network on a set of simulations that included increasing, decreasing, and constant trend populations. We did not provide the network any information about population trend beyond what it could infer from the input images. The range of trends in the training set is conceptually similar to a prior distribution, in that the network is expected to work best when the true trend lies within the "prior" range. We do not ask the network to also infer trend: indeed, the network might be either effectively learning the trend and adjusting accordingly, or learning to use patterns that are unaffected by the trend (or both). The updated network estimated population size to within about 10% of the true value for all population trends and sampling biases (Table 4). This robustness comes at little cost – it was much more accurate than when

CKMRnn performance for unknown population trend			
Population trend	Spatial sampling bias	Mean relative absolute error	Mean relative error
decreasing	uniform	0.110	0.065
constant	uniform	0.109	-0.002
increasing	uniform	0.116	-0.093
decreasing	medium	0.108	0.056
constant	medium	0.099	-0.020
increasing	medium	0.109	-0.085
decreasing	high	0.122	0.078
constant	high	0.105	0.011
increasing	high	0.099	-0.064

Table 4. CKMRnn performance on datasets with mixed population trends, using a single network trained across a range of trends. Both training and test sets are simulations with population size increasing or decreasing by 1% per year or constant population size.

trend was misspecified but only slightly less accurate than when trend was perfectly specified. Errors still tended to be positive for decreasing trend and negative for increasing trend, but only slightly (Figure 4).

2.3.2 African elephants. The African elephant dataset contains genetic information from 256 dung piles [25]. These samples are concentrated on the outer edges of Kibale National Park, with few samples from the middle, suggesting that there is strong spatial bias in sampling (Figure 1). The dung samples contain 124 unique individuals, 103 of which were not recaptured, 16 were captured on two different days, 1 on three different days, 3 on four days and 1 on five days. Distances between subsequent recaptures ranged between 0.54 km and 33.94 km, with an average distance of 9.32 km and an average distance per day of 0.79 km. We plotted these recapture histories for input to the neural network by connecting subsequent recaptures of the same individual on different days with line segments, resulting in 47 line segments (Figure 1).

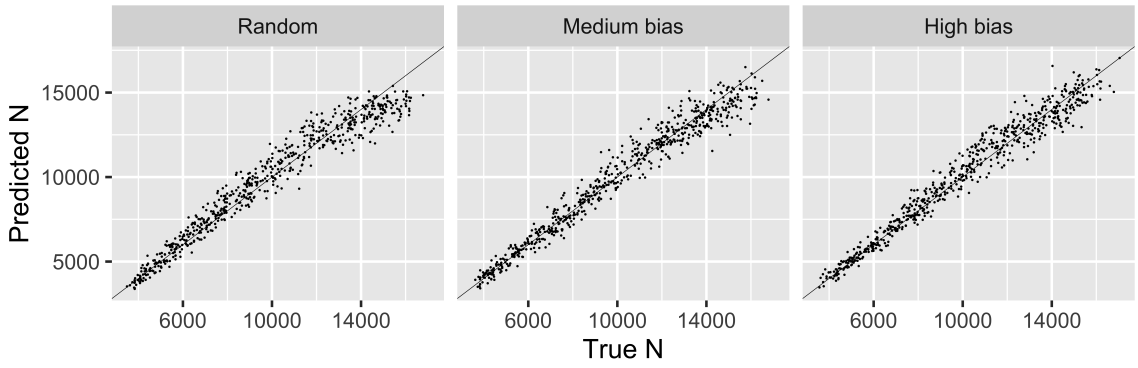

(a) True vs predicted N for three levels of spatial sampling bias. y = x line included for reference.

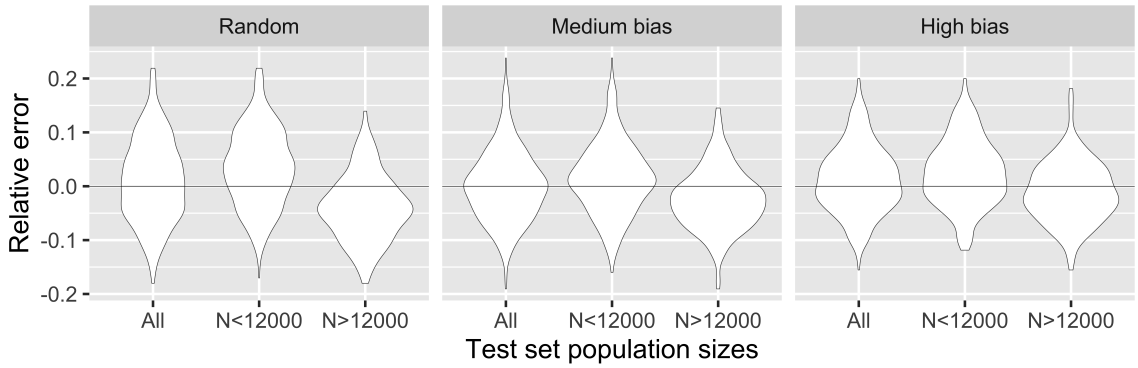

(b) Relative error for three levels of spatial sampling bias and three test sets: all simulations, simulations with $N < 12000$, and simulations with $N \geq 12000$.

Figure 2. Performance of CKMRnn when trained and tested on simulations with constant population size over time.

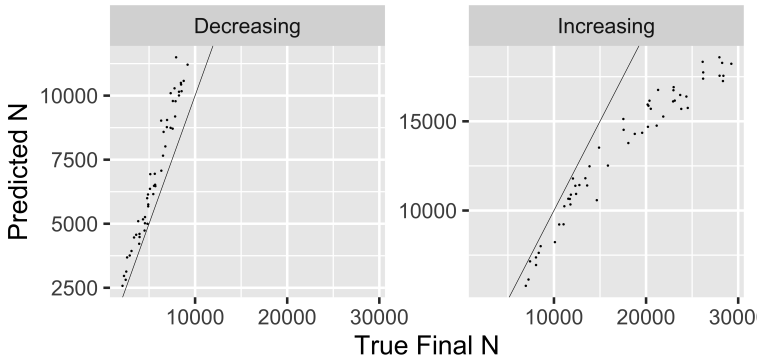

(a) True vs predicted N for population sizes increasing or decreasing by 1% per year. y = x line included for reference.

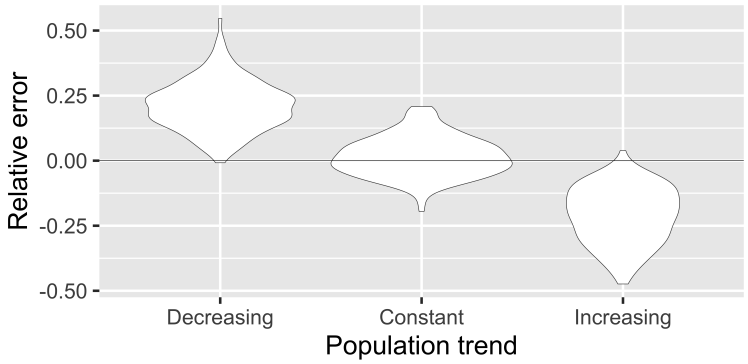

(b) Relative error for increasing, decreasing, or constant population size test sets.

Figure 3. Performance of CKMRnn when trained on simulations with constant population size over time and tested on simulations with increasing, constant, or decreasing population size. All results are for medium spatial sampling bias.

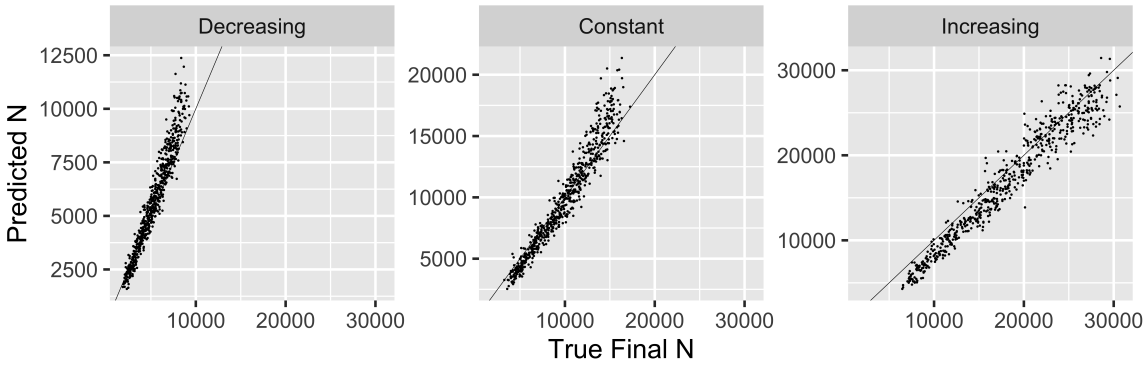

(a) True vs predicted N for population sizes increasing or decreasing by 1% per year or constant. y = x line included for reference.

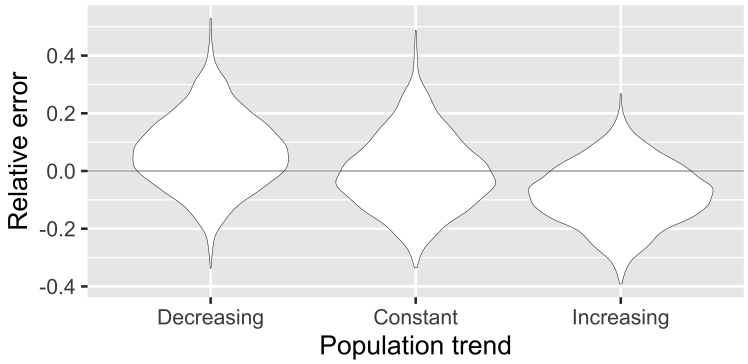

(b) Relative error for increasing, decreasing, or constant population size test sets.

Figure 4. Performance of CKMRnn when trained and tested on simulations with increasing, constant, or decreasing population size. All results are for medium spatial sampling bias.

Among the unique individuals, there were 260 parent-offspring pairs. The distance between parent and offspring sampling locations ranged from 0 to 47.12 km, with an average of 17.84 km. Some of the individuals in the pairs were captured multiple times. We plotted these parent-offspring pairs for input to the neural network by treating samples from the same individual on two different days as unique individuals, resulting in 338 line segments, shown in Figure 1.

To validate the method in this system, we first tested the performance of CKMRnn on simulated elephant populations by training the network on 7500 simulations and testing on the remaining 2500. The neural network performed very well on the held out test set. Estimates were unbiased and estimated population size was on average within 12.3% of the true value for population sizes between 100 and 1500 (Figure 5). The variation in estimates increased somewhat as population size increased (Figure 5a). This is expected because sample size relative to population size decreases as population size increases.

Finally, we used our trained network to estimate population size in Kibale National Park from images of empirical sampling intensity, recaptures, and parent-offspring pairs, obtaining an estimate of 450 elephants. To produce a confidence interval, we generated 500 parametric bootstrap replicates by simulating 500 populations each with population size 450, then used the network to estimate population size for each replicate to get a bootstrap distribution (Figure 6). The 95% confidence interval based on the distribution is $(323, 620)$.

For comparison, we ran a traditional capture-recapture analysis of the elephant dataset to estimate population size. We used a log-linear model in the R package `Rcapture` [5]. Based on AIC scores, the best closed population, continuous time model was Chao's Lower Bound with heterogeneity in capture probability between

individuals [46]. The estimated population size was 454.1 with a 95% CI of (316.3, 752.9).

There are two previous estimates of population size in Kibale, a 2021 cut-transect survey estimate of 566 elephants with a 95% CI of 377 to 850 from Daniel, Edward and Kennedy [17] and the 2025 capture-recapture estimate of 573 elephants with a 95% CI of 410 to 916 from Goodfellow et al. [25].

Our CKMRnn estimate is notably smaller than the estimate of 573 obtained by Goodfellow et al. [25] using the same capture-recapture data, but still falls within the 95% confidence interval of this estimate. This difference in estimates is likely due to differences in the way we accounted for non-independence between sampling locations. Goodfellow et al. [25] accounted for non-independence by filtering the data to include only one capture instance for individuals with multiple captures near the same sampling location. We accounted for non-independence using a much less strict filtering process (only filtering captures of the same individual on the same day), and then accounting for the remaining non-independence through simulation of the sampling plan.

2.4 Discussion

In this paper we develop a spatially explicit close-kin mark-recapture method, CKMRnn, that uses a convolutional neural network (CNN) to estimate population size from maps of sampling intensity, kin pairs, and other relevant information such as recaptures. Our method is accurate and robust, even for populations with limited dispersal and spatially biased sampling, a situation in which most previous methods are biased [15, 51]. On simulated test populations with spatial population structure and spatially biased sampling, CKMRnn was unbiased and estimated true population size to within 6% of the true value when population trend was constant over time and

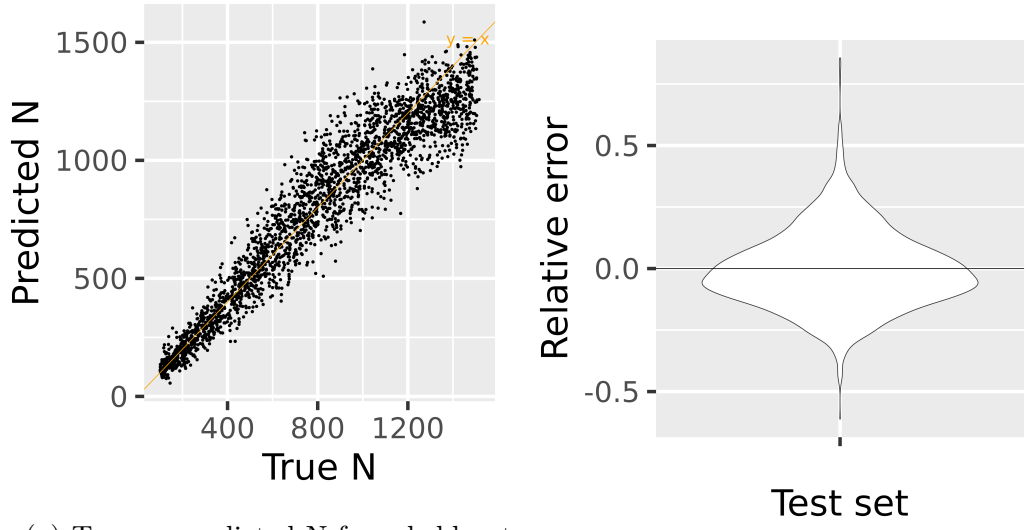

(a) True vs predicted N for a held out test set of elephant simulations. y = x line included for reference.

(b) Relative error for a held out test set of elephant simulations.

Figure 5. Performance of CKMRnn on elephant simulations.

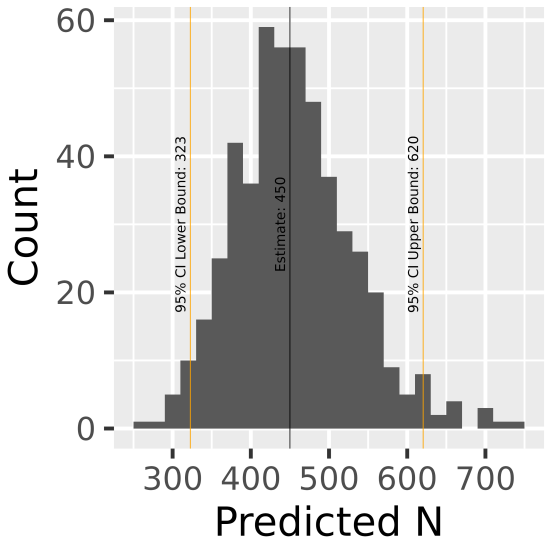

Figure 6. Histogram of parametric bootstrap replicates for population size of African elephants in Kibale National Park. Vertical lines are the point estimate and bounds of the 95% confidence interval.

to within about 10% when population trend was unknown. CKMRnn also performs well on empirical data. We used CKMRnn to estimate population size of elephants in Kibale National Park in Uganda from recaptures and parent-offspring pairs. We estimated that there are around 450 elephants in the park, with a 95% confidence interval of 323 to 620. The estimate very closely agrees with estimated population size using a traditional capture-recapture method and has a 32% narrower confidence interval.

CKMRnn has several advantages over previously-developed spatial and simulation-based CKMR methods. For instance, the spatial methods developed by Sévêque et al. [51] use a pseudo-likelihood-based approach to account for spatially biased sampling. This approach is limited to simple models of spatial population dynamics. For example, it assumes that dispersal distances are independent between individuals and that the sampling location of a female is the initial location of the offspring. In addition, the pseudo-likelihood approach assumes sampled pairs are independent and so is best suited to systems where population size is large relative to sample size. Relaxing such assumptions is difficult in the likelihood setting because analytical expressions for observing kin pairs quickly become hard or impossible to write down. Because CKMRnn instead relies upon simulation, the complexity of the model is limited only by our ability to simulate it. Our elephant example demonstrates how this flexibility allows us to apply CKMR to populations that violate the assumptions made by likelihood methods. In the small elephant population, sampled pairs are not independent, and we are able to account for this non-independence by simulating it. Juvenile elephants stay with their mothers for many years before dispersing, and we are able to account for this pattern by explicitly simulating the movements of mothers and juveniles. In the future, we plan to extend

CKMRnn to account for even more complex dynamics such as correlated movement of closely related individuals in kin groups.

Other researchers have also implemented simulation-based methods. For instance, the simulation-based methods developed by Conn [14] use Approximate Bayesian Computation (ABC) to infer population size. The observed data for this ABC method are counts of kin pairs grouped by relevant information such as age class. This ABC method works well, but it does not directly account for spatial information. Each sampled individual has a unique location on the landscape, and so when pairs of individuals are aggregated into groups to use as observed data for the ABC method, these unique locations are lost. Our CNN, which relies on an image-based input format that includes the spatial locations of all samples, thus has the potential to take advantage of spatial information.

Currently, there are three major limitations of CKMRnn: (1) it does not explicitly include information about time; (2) it estimates a single population density rather than a map of density that varies across the landscape, and (3) it assumes that kin identification is without error. We believe that CKMRnn could be extended to relax these assumptions, but will leave this for future work.

In pseudo-likelihood methods, time is included in the model through ages of sampled individuals and through information about sampling time. In these methods, both parent-offspring and half-sibling pair probabilities are computed based on the birth year of the potential offspring or the birth years of the potential half-siblings [12], and so ages of sampled individuals are required and error in aging can cause bias in abundance estimates [45, 55]. Observing ages and sampling times also allows these methods to estimate parameters such as survival and population trend. CKMRnn does not use ages of individuals as input to the network, and assumes that the age

structure of the population is known (since this is used in setting up the simulation). In Kibale, the available samples are from only one year and age of the sampled individuals is unknown, and so we do not have much information about parameters that depend on time, such as survival or population trend. Elephants are also fairly well studied, and so we have prior information on the age structure and survival dynamics of elephants. However, for populations that are sampled yearly such as through hunter harvests, or for populations that are not as well-studied as elephants and so age structure and survival is unknown, we would want to incorporate age and time information. Future work to include time might vary age-dependent survival parameters in the training simulations and/or adapt the network architecture to take as input age and sample time information. Such networks might also estimate parameters such as survival and trend in addition to population size.

Our applications here have assumed that the population is closed and that population density is roughly constant across the landscape. Most populations, including the Kibale elephants, do not meet these assumptions. Despite these assumptions, CKMRnn was able to get reasonably accurate estimates for Kibale, however, for populations with greater variation in density across the landscape or higher levels of immigration and emigration, we would likely need to relax these assumptions. For example, in populations without clear boundaries, estimating a single, closed population size is not meaningful [48]. In addition, population density that varies across the landscape influences patterns of kin pairs and needs to be accounted for. Previous methods such as that from Sévêque et al. [51] account for varying density by assuming that the relative density of individuals across the landscape is known from auxiliary data such as camera traps. If auxiliary data was available, this approach could easily be incorporated into CKMRnn by either

holding it fixed (as for our simulated elephants, who only live within the park), or adding a map of relative density to the training simulations. If auxiliary data were not available, one could use our approach by varying maps of relative density in the training simulations, which we would expect simply to increase uncertainty in the estimated population sizes. One especially exciting future direction is to extend CKMRnn to directly estimate ecological parameters. For example, we can add a relationship between forest cover and population density to our simulation, and then estimate the parameters of this relationship. Spatially explicit capture-recapture models are already able to incorporate these ecological parameters [48].

Finally, in this paper we assumed that there was no uncertainty in identifying kin pairs. Bravington, Skaug and Anderson [12] describe two ways of accounting for uncertainty, first, by adding a false negative rate for kin pair estimation to the model and then estimating this rate along with other parameters, and second, by treating kinship as a latent variable and using genetic data as the observation. Both of these approaches could be adapted to account for uncertainty in identifying kin pairs in CKMRnn. For example, we can add a false negative rate for each kin relationship to the training simulations. Or, for populations with significant inbreeding or population structure that influences accuracy of kin identification, we can simulate genotypes of individuals, and then use these genotypes to estimate kin and generate training images. It might even be possible to follow previous methods that use neural networks to estimate other population parameters [52, 53, 54] and use genotypes directly as input to the network.

A natural question in application of CKMRnn is: how accurate does the simulation need to be? Implementing an individual-based spatial simulation can be daunting, as it requires specification of many behaviors, such as mate-finding

and dispersal, that may not be well-understood. For a recent, comprehensive guide to implementing spatial simulations, see Chevy et al. [13]. Clearly, no simulation can perfectly capture the precise demographic dynamics of a given species, so some degree of approximation is necessary. This is not unique to simulation-based inference: similarly, any analytical method makes a variety of assumptions about the underlying model (and, these assumptions are often less obvious). As we've demonstrated here using population trend, robustness to uncertainty in model parameters can be trained directly into CKMRnn by simulating across a range of parameters in training data. Which aspects of demography are important to model and how model uncertainty affects accuracy of estimates are empirical questions that will depend on the system being studied.

Some aspects of uncertainty are, however, unavoidable. Similar to how individual heterogeneity in capture probability leads to nonidentifiability in mark-recapture estimates [46], variation in offspring number distribution can lead to nonidentifiability in CKMR estimates of population size, at least for nonspatial models [31, 36]. The distinction is related to "effective" versus "census" population size, N_e versus N [60]. One definition of N_e is in terms of the proportion of pairs that are siblings, and so two populations having the same sibling density may have the same N_e but different N. To the degree that a CKMR method relies on sibling density, therefore, it may be N_e rather than N that is estimable and so different models with the same N_e but different N may be difficult or impossible to distinguish. CKMRnn predicts N, not N_e (because that is what it is given for training data), but in some situations N_e might be more accurately estimable. Information about N beyond N_e comes from two sources: from "prior" information about the demographic model (i.e., how the simulation is coded), and from time-varying data (e.g., mark-recaptures or parent-

offspring relationships). Better understanding of these aspects could improve future study design and interpretation.

Many parts of the CKMRnn pipeline are specific to the population being studied, and so we do not provide an R or python package that can be directly applied to a new system. Much of the code we used to run CKMRnn on the Kibale elephants can be adapted for a new system, and we provide this code as well as instructions for running it in the CKMRnn GitHub repository. The most challenging step in applying CKMRnn to a new system will likely be writing a reasonably accurate simulation of the population and sampling plan. The pipelines we provide for finding and visualizing kin pairs and recaptures and generating training simulations could be directly used with very few changes. We also provide a pipeline for training the network and obtaining estimates and parametric bootstrap confidence intervals. This pipeline can also be directly used with few changes, but requires access to a GPU.

In summary, we have found that our new method, CKMRnn, has the potential to improve monitoring for many terrestrial species, which often have population structure and spatially biased sampling. We expect CKMRnn to be especially useful for populations such as the Kibale elephants where individuals are elusive and hard to capture.

Code and data are available at `https://github.com/giliapatterson/CKMRnn`.

BRIDGE

In Chapter II, I developed a spatially-explicit, simulation based method for inferring population size from close-kin. I demonstrated that the method is unbiased when dispersal is limited and sampling is spatially biased, and that the method is robust to unknown population trend. I also demonstrated that the method has the potential to improve estimates of population size in African elephants by using both kin pairs and recaptures. However, I used the elephant data only as a proof of concept and did not accurately measure all sources of uncertainty. In Chapter III, I extend the methods to account for two of these sources: uncertainty in estimated kin relationships and social group structure. I then explore the feasibility of implementing CKMR in the Kibale elephants by determining the expected error in population size estimates for the original number of sequenced microsatellites and for a hypothetical dataset with many more sequenced microsatellites.

CHAPTER III

ESTIMATING POPULATION SIZE IN AFRICAN ELEPHANTS WITH SIMULATION-BASED SPATIALLY EXPLICIT CLOSE-KIN MARK-RECAPTURE

This chapter is coauthored with Silas Tittes, Nelson Ting, and Peter Ralph. Nelson Ting provided input on the elephant simulation model. Silas Tittes ran the `CKMRsim` analyses for measuring error in kin estimation and implemented the kin estimation method. I performed all other analyses and wrote the manuscript.

3.1 Introduction

Non-invasive genetic data are a powerful tool for monitoring populations of conservation concern. The most common method for using this data to estimate population size is genetic capture-recapture, which identifies when the same individual has been sampled multiple times and uses these recaptures to estimate population size. [38, 41]. Another, more recently developed method, called close-kin mark-recapture (CKMR), uses genetic data to identify close-kin pairs in a sample, such as parents and offspring, and uses these similarly to recaptures to estimate population size [12, 32]. CKMR is very promising for improving population monitoring. Because CKMR does not require recaptures, it can be used for species that are lethally sampled or that are highly elusive and hard to recapture. And because it uses more information from a genetic sample than simply identifying recaptures, CKMR can potentially be combined with capture-recapture to improve estimates.

CKMR methods have been successfully used in several species; however, CKMR methods do not yet model the complex spatial, social, and reproductive dynamics of many populations. These complexities are both a source of information and of bias. Because the probability two individuals are kin will be higher in areas with lower

population density than in those with higher density, modeling the spatial locations of kin pairs can provide information on local population density [10]. Incorrectly specifying the relationship between age and length [45, 55], incorrectly modeling breeding dynamics, such as assuming monogamy when the population is actually polygynous, [50], or assuming a simple random sample from the population when there is high spatial bias in sampling and limited dispersal [15] can lead to bias in population size estimates.

Most applications of CKMR to date use likelihood-based methods (except [14]). One challenge in these methods is that accurately modeling complex population dynamics can cause likelihoods to become difficult or intractable to compute. Simulation-based methods are a promising way of overcoming this challenge because they are limited only by the ability to simulate an approximation to the system. In Chapter II, we developed a simulation-based method for close-kin mark-recapture to model spatially biased sampling and limited dispersal. In this chapter, we extend the method to model the complex social structure and reproductive dynamics of a population of elephants in Kibale National Park in Uganda.

Kibale National Park is a protected area in the Albertine Rift in southwestern Uganda near the border with the Democratic Republic of the Congo. Kibale protects a population of elephants that are primarily hybrids of savanna (*Loxodonta africana*) and forest (*Loxodonta cyclotis*) elephants [25]. These elephants have experienced habitat loss, poaching, and intense human conflict over the past few generations and likely went through a severe population bottleneck about 50 years ago. Monitoring elephants in Kibale is time and labor intensive and so we know very little about the dynamics of this population of hybrids. We have two recent population size estimates for Kibale, both from labor-intensive sampling plans. The first is a 2021

cut-transect survey that estimated population size to be 566 with a 95% confidence interval of 377 to 850 [17] and the second is a 2025 capture-recapture estimate based on non-invasive sampling from dung that estimated population size to be 573 with a 95% confidence interval of 410 to 916 [25]. Close-kin based methods combined with capture-recapture data could potentially improve these estimates. However, current CKMR methods, including our simulation-based method, do not account for the complex social dynamics of elephants.

In this paper, we explore opportunities for using kin-based methods for population monitoring of elephants. We: (1) develop an accurate model of elephants in Kibale National Park, including matrilineal social structure, to test methods for population monitoring from genetic data; (2) extend the methods of Chapter II to account for uncertainty in kin estimation; (3) measure the effect of number of sequenced loci on uncertainty in kin estimation and in CKMR estimates of population size; and (4) determine the feasibility of using CKMR methods to monitor elephants in Kibale.

3.2 Methods

In this paper, we analyze the same genetic dataset for elephants in Kibale National Park in Uganda as in Chapter II. The dataset consists of 256 genetic samples from dung piles across Kibale. 14 microsatellites were sequenced for each sample and used to identify recaptures. The dataset was collected by Claire Goodfellow and collaborators [25, 26].

Our methods build on the simulation-based methods in Chapter II and have four main steps. First, we developed and parameterized an individual-based, spatially explicit, genetic simulation of the elephant population in Kibale and the sampling plan used to collect the genetic dataset. We developed the simulation in the program

SLiM [29], and parameterized social structure, mate choice, reproduction, dispersal, and mortality based on previous studies of forest and savanna elephants. We then implemented a simulated sampling plan that closely follows the sampling plan from Kibale National Park. Second, we explored error rates for kin estimation and estimated kin pairs for both the empirical and simulated samples. Third, we used our simulation to train the neural network from Chapter II to estimate population size from kin pairs. We then tested the accuracy of the network on simulated test datasets with varying numbers of microsatellites. Finally, we applied our network to the empirical data from Kibale to estimate a population size and 95% confidence interval.

3.2.1 Individual-based simulation model. We modeled the population of elephants in Kibale using an individual-based genetic simulation implemented in the simulation software SLiM [29] and parameterized the model to represent the population of elephants in Kibale as closely as possible. The simulation takes place in continuous space on a map of Kibale, meaning that individuals can occupy any location on the landscape and are not limited to a discrete set of grid cells or points. The model simulates discrete time steps, each representing a year. In each year, individuals have the opportunity to mate, reproduce, disperse, and die, with the dynamics of each incorporating the social structure, mating system, fertility, movement, and mortality of elephants.

Social structure. Both savanna and forest elephants have a complex, matriarchal social structure, and adult females and their sub-adult offspring form groups of individuals that move together [3]. These groups tend to be formed of closely related individuals, and so modeling their dynamics is important for accurately modeling the distribution of close kin on the landscape.

The elephants in Kibale are primarily hybrids of savanna and forest elephants, with some savanna elephants and very few forest elephants [25]. Because there is very little information about the social structure of this mixed population, we modeled a social structure that falls between savanna and forest elephants. Social dynamics have been far more extensively studied in African savanna elephants than forest elephants. In savanna elephants, groups are hierarchical, with multiple mother-offspring units forming kinship groups and multiple kinship groups forming clans of 50 to 250 individuals that gather during the dry season. Females within kinship groups tend to be significantly related to each other, but occasionally groups contain an unrelated, immigrant female who likely joined after her relatives died [3]. Forest elephants likely form much smaller groups, with sizes around 3 individuals. Females within a group tend to be related to each other, but this pattern is not as strong as in African elephants. Forest elephants also likely have more movement of individuals or mother-offspring pairs between groups. This is called an individual-based fission-fusion society [3].

To model social groups in our simulation, we kept track of a separate list of locations and sizes of social groups. Each individual adult female elephant in the simulation is assigned a social group, and her movement and the movement of her juvenile offspring is determined by the movement of the social group. Each year, we modeled splitting and merging of groups based on their locations and the number of adult female members in the group.

The average adult female size of groups in the population is controlled by a single parameter, Γ. At the beginning of the simulation, the population is initialized with $N_{\text{initial}}/\Gamma$ groups, where N_{initial} is the initial number of individuals in the population, and each female and juvenile male is randomly assigned to a group. In this initial

step, juveniles do not have a mother and so are assigned a social group. After the initial step, new offspring are not assigned a social group and instead follow their mother until maturity.

It is thought that the distribution of resources across the landscape plays a role in the social dynamics of elephants, with smaller, more flexible groups when resources are spread out, such as in forest ecosystems, and larger, more cohesive groups when resources are clustered and seasonal, such as in savanna ecosystems [3]. Since Kibale is primarily forested, we chose to model the social dynamics of hybrids with a more flexible group structure than savanna elephants. In our simulation, we modeled social group dynamics to approximate an individual-based fission-fusion society by setting rates of group fission and fusion as in Gueron and Levin [28]. Each generation, each social group has an opportunity to split into two new groups and to merge with neighboring groups. For splitting, each group with more than 1 member splits with probability $\beta/\left(1+\mathrm{e}^{-4(N_{\mathrm{group}}-\Gamma)}\right)$, where N_{group} is the number of adults in the group. If the group splits, the number of adult members in the new group is chosen uniformly randomly from 1 to $N_{\mathrm{group}}-1$ and the members of the new group are chosen randomly from the adult members of the current group. For merging, each group with at least one other group within 0.5 km randomly chooses one of these neighboring groups for a potential merge. The two groups merge with probability $\alpha/N_{\mathrm{current}}N_{\mathrm{neighbor}}$, where N_{current} and N_{neighbor} are the adult size of the current and neighbor groups, respectively.. If the groups merge, all individuals from the current group move to the neighbor group and the current group is eliminated. Each generation, we also eliminate groups that are empty due to mortality of all adult members.

Juveniles are not assigned a social group and instead always follow their mother. If their mother dies, they are assigned a new mother by choosing from all mature

females in the population weighted by relatedness to the juvenile. When an individual reaches maturity, females are assigned to the social group of their mother and males leave the social group to disperse independently. In one population of forest elephants, both males and female were found to be able to leave their natal group at a median age of 15 [59], and we chose to use this age as the age of maturity in our simulations.

In both savanna elephants and forest elephants, males occasionally associate with other males or with female groups [3]. We chose to ignore these male social groups both for simplicity and because forest elephants are thought to have fewer associations than savanna elephants. In our simulation, males range solo and their movement is independent of other individuals.

Mating and reproduction. In both forest and savanna elephants, females are only fertile every 4-5 years, and the probability a female is fertile varies based on her age and the amount of time since she last reproduced. Because fertile females are rare, males show fierce competition for the available females [3]. Males that are larger, older, and in a state of heightened testosterone called musth tend to be more likely to mate with a female. Because females are a rare resource that is hard to find, there is also an element of luck [3].

In studies of both forest elephants in Dzanga Bai, Central African Republic and savanna elephants in Samburu, Kenya, female fertility was relatively constant between ages 23 and 49, with fertility increasing linearly from age 10 to 23 and decreasing linearly after age 49 [59, 62]. In Dzanga Bai, the youngest females to reproduce were 10 and the oldest 60 [59]. Fertility was slightly lower in Dzanga Bai than in Samburu, with fecundity of about 0.07 offspring per year for females age 23-49 in Daznga Bai compared to about 0.12 for Samburu. For Dzanga Bai, the reproductive value for females, that is, the expected number of offspring she will produce across

her lifespan, was about 1.5 for individuals of age 0, peaked at 1.75 for individuals of age 15, and then declined to 0 around age 60.

In our simulation, we modeled female fecundity by computing the probability a female reproduces based on both age and time since last offspring. The model is controlled by a single parameter, $P_{\max}$, that is the maximum probability a female reproduces. For females that have not reproduced in many years, the probability of reproduction increases linearly from 0 to $P_{\max}$ for ages 10 to 22, is $P_{\max}$ for ages 23 to 49, and decreases linearly from $P_{\max}$ to 0 for ages 50 to 60. To model long gestation and lactation periods, these probabilities are multiplied by gap factor $1/\left(1+\mathrm{e}^{-2(g-5)}\right)$, where g is the number of years since the female last reproduced. The gap factor increases from 0 to 1, with a value of 0.5 at gap 5.

If a female is fertile, she chooses a mate from males of reproductive age that are within 10 km of her current location. We set the minimum age of reproduction for males to be 25. If at least one male is available, she chooses a mate with the probability each male is chosen proportional to his age. She then produces one offspring and this offspring is placed in a separate population representing fetuses. After 2 years, if the mother is still alive, the offspring is moved to the main population and remains with the mother until maturity or until the mother dies.

Because the probability a female reproduces depends on both the gap since she last reproduced and the availability of reproductively mature males to mate with, the relationship between the parameter $P_{\max}$ and realized fertility and reproductive value is not straightforward. So, to determine the value of $P_{\max}$, we ran simulations with varying $P_{\max}$, computed realized fertility and reproductive values in the simulations, and chose $P_{\max}$ so that simulated female fertility probabilities fell between measured fertility probabilities for forest elephants in Dzanga Bai [59] and savanna elephants

in Samburu [62]. To calculate fertility and reproductive value, for each year after a burn-in period of 50 years, for each female alive in that year, we recorded whether or not the female reproduced and her age. For fertility at age a, we computed the proportion of females of age a that reproduced. For reproductive value at age a, we filtered the recorded females to include only those who were a years old at some point after the burn-in period, then for each of these females, computed the total number of offspring they produced at age greater than or equal to a. Reproductive value is then the mean of these totals.

The realized reproductive values include the effect of both age-based survival curves and density dependence, and so we expect them to be different than the theoretical reproductive values based only on age-dependent survival. To measure the size of this effect, we computed Fisher's reproductive value at each age based on realized fertility and age-dependent survival [22]. Fisher's reproductive value for a simulated female elephant of age a is

$$\sum_{y=a}^{70} (\ell_y/\ell_a)\, m_y$$

where ℓ_a is the probability a female survives to age a and m_a is the fertility of a female of age a.

Movement and dispersal. Both savanna and forest elephants have complex patterns of movement and dispersal that are influenced by factors such as the availability of resources, human activity, season, and the individual elephant's preferences and sex [7, 8, 63]. Because we do not have much information on the movement of elephants in Kibale and because detailed movement models are likely unnecessary to get accurate population size estimates, we greatly simplified these dynamics in our simulation.

Our simulation models elephant movement yearly for the first 199 years of the simulation and daily during the 200th year. For yearly movement, adult females move with their social groups, juveniles move with their mothers, and adult males move independently. We set yearly movement for males to 12 km and for females to 9 km, roughly consistent with the yearly home range sizes of 238 km^2 for males and 135 km^2 for females found by Beirne [7] for forest elephants in Gabon. Each social group moves 9 km per year on average, with the new position drawn from a bivariate normal distribution around the current location. Adult females within a social group are assigned the position of the social group plus a small amount of noise (0.2 km on average), and juveniles are assigned the position of their mother, plus a small amount of noise (0.2 km on average). For daily movement, social groups move an average distance of $(1/365) \cdot 9 = 0.025$ km per day for 365 days, with adult females again following social groups and juveniles following mothers. Yearly and daily movement of adult males follows the same pattern, but with average distance of 12 km per year and $(1/365) \cdot 12 = 0.033$ km per day.

Kibale National Park has both forested and savanna sections, and these different habitats likely influence elephant dispersal and movement; however, we did not model this variation and in our simulation dispersal is equally likely to all points inside the park. To prevent dispersal outside of the park, when a social group or adult male chooses a new location, we check if the new location is inside the park and if not, choose another location. This process is repeated until a location within the park is found or until 20 tries. If no location within the park is found in 20 tries, the individual or group stays at its current location.

Mortality. Forest elephants have much lower mortality than savanna elephants, especially as juveniles, likely because of the absence of drought and

predators in forest ecosystems compared to savanna ecosystems [59]. Because Kibale is primarily forested, we chose to model age-dependent survival based on forest elephant demographic parameters estimated by Turkalo, Wrege and Wittemyer [59] for Dzanga Bai in the Central African Republic. In this population, mortality was very low ($< 3\%$) for individuals younger than age 13. After age 13, male mortality increased relative to female mortality, with females about twice as likely as males to survive to a given age. Males had a maximum lifespan around 65 years and females around 70 years [59].

In our simulation, we modeled survival as a combination of age-dependent and density-dependent survival. For the age dependent survival component, we set the probability of survival to each age to approximate the survival probabilities from Turkalo, Wrege and Wittemyer [59]. We then converted these unconditional probabilities to the conditional probability that an individual of age a survives to age $a+1$. Both conditional and unconditional probabilities are shown in Figure 7. For the density dependent survival component, we set a carrying capacity K and multiplied the age-dependent survival probabilities by K divided by current population size. The density dependent component ensures that the population remains relatively stable around size K. We varied K to simulate populations of different sizes.

Microsatellites. The elephant genetic dataset from Kibale contains only 14 microsatellites, limiting our ability to accurately infer kin pairs. To model this uncertainty in kin pair identification, we simulated 14 microsatellites with the same frequencies as the empirical dataset. To do this, we followed the microsatellite vignette in the SLiM manual [29]. Each individual in the simulation has two genomes with 14 positions each, each position representing one microsatellite locus from the empirical dataset. To accurately simulate the empirical allele frequencies, for each initial

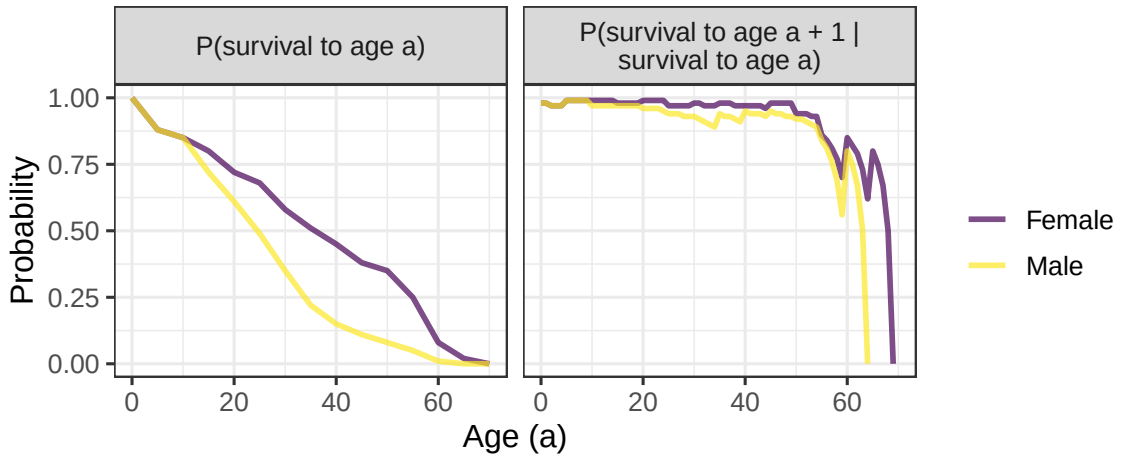

Figure 7. Age-dependent survival probabilities for simulated elephants. The unconditional probabilities of survival to each age (left figure) were taken from Turkalo, Wrege and Wittemyer [59], then converted to conditional probabilities of survival to the next year (right figure).

individual in the population, the number of repeats at each position in each genome is drawn from the empirical repeat counts at that locus following the frequencies in the empirical dataset. As the simulation proceeds, offspring inherit their genomes from their parents with free recombination between positions. Genomes accumulate mutations at a per generation per site rate of 10^{-4}, and a mutation randomly adds or subtracts a single repeat.

To explore the effect of increasing the number of sequenced microsatellites on estimates of population size, we also ran simulations with a hypothetical dataset with 56 microsatellites. The 56 microsatellites consisted of 4 copies of the original 14 sequenced microsatellites.

Sampling. The samples in Kibale were taken by rotating through a grid of potential sampling locations each week and collecting fresh dung samples found around the sampling location [25] . A total of 256 samples were collected on 49 days.

One limitation of this dataset is that we do not have information about sites visited by the field team where no dung was found.

We modeled the sampling scheme and the lack of information about absence of dung as closely as possible. We first created a grid of 1 km by 1 km grid cells overlaying the map of Kibale, and set the potential sampling locations to be the center of the grid cells. Sampling takes place in year 200 of the simulation on the same 49 days when sampling took place in the empirical data. On each of the 49 sampling days, we randomly selected a site from the potential locations and sampled all individuals within 1 km of the sampling site. If too few samples were obtained, we randomly selected a neighboring site and sampled all individuals within 1 km of the new site. On the ith sampling day, we repeated this process until at least $(256/49)i$ samples were collected total or at least 50 sites were visited, whichever came first. If sampling all of the individuals within 1 km of a site would cause the total sample size to exceed 256, we downsampled the individuals to reach 256 exactly. If at the end of the 49 sample days less than 256 individuals were sampled, we randomly sampled individuals from the population to reach a sample size of 256.

3.2.2 Kin estimation. We estimated parent-offspring, half-sibling, and full-sibling kin relationships for both simulated and empirical data through a likelihood-based approach. Our approach has two steps. First, we distinguish between unrelated and related pairs by computing the log-likelihood ratio for parent-offspring to unrelated and calling all pairs with a ratio below a set cutoff as unrelated. For pairs above the cutoff, we compute the likelihood of parent-offspring, half-sibling, and full-sibling, and call the pair the relationship with the highest likelihood. We used the R package `CKMRsim` to compute all likelihoods [1].

Changing the likelihood ratio cutoff changes the specificity and sensitivity of kin estimation. When the log-likelihood ratio cutoff is increased, the probability a true kin pair will be estimated to be kin increases (higher sensitivity), but the number of unrelated pairs identified as kin also increases (lower specificity). To explore the effect of the cutoff, we used Mendelian inheritance simulations implemented in the `CKMRsim` package [1]. We generated two sets of simulations, one with 14 microsatellites with the same allele frequencies as the empirical data and one with 56 microsatellites composed of four copies of the 14 empirical microsatellites. For each set, we simulated genotypes for 10000 pairs each of parent-offspring, full-sibling, half-sibling, and unrelated. We then estimated the relationship of each pair using different log-likelihood ratio cutoffs.

Because we are using kin pairs as a source of information about population size, we did not choose a fixed log-likelihood ratio cutoff. Instead, we generated several sets of training data using different log-likelihood cutoffs and chose the cutoff that gave the best predictions of population size. This step is described in more detail in section 3.2.3.

3.2.3 Neural network training and testing.

Neural network architecture. To estimate population size, we adapted the convolutional neural network (CNN) from Chapter II. CNNs are a type of network designed to extract information from images. Our CNN takes as input images of parent-offspring pairs, half- and full- sibling pairs, sampling locations, and, optionally, recaptures, and outputs a single population size. For examples of the input images and further details on how they are produced, see Figure 1 and Section 2.2.1. We chose to use a CNN rather than other statistical models because it allows us to use images directly as input. Other methods, such as Approximate Bayesian Computation (ABC), would require us to convert the spatial locations and kin pairs to summary

statistics, potentially losing some of the information about population size contained in the data.

The CNN has 4 layers, two convolutional layers that extract features from images and 2 fully connected layers that convert these features to a single population size. The first convolutional layer takes as input the kin, sampling, and, optionally, recapture images (3 or 4 837 pixel by 566 pixel images) and outputs 8 419 pixel by 283 pixel images, and the second layer takes these images as input and outputs 16 210 pixel by 142 pixel images. These images are then collapsed into a single vector, with each pixel of each image corresponding to a single element of the vector. The first fully connected layer takes as input this vector and outputs another, smaller, vector with dimensions 1024 by 1, and the final fully connected layer processes this vector into a single population size.

The network architecture has fewer parameters than the architecture from Chapter II. We found that this smaller architecture performs as well as the original, but requires less memory and time to train.

Training dataset. We trained the neural network using the Kibale elephant simulations. To generate the training dataset, we ran 10000 simulations and recorded the genotypes, individual identifications, locations, and sampling times of sampled individuals and the final population size for each. We varied final population sizes by drawing the carrying capacity, K, for each simulation from a uniform distribution between 100 and 1500.

The information we have about simulated sampled individuals matches the data we have for the empirical samples from Kibale, and we processed both simulated and empirical data in exactly the same way. We first filtered the data to exclude samples of the same individual on the same day. We then estimated parent-offspring, half-

sibling, and full-sibling relationships with each potential log-likelihood ratio cutoff. For each sample and each cutoff, we created images of parent-offspring pairs, half- and full- sibling pairs, recaptures, and sampling intensity. The parent-offspring and sibling images were created by connecting the sampling locations of each individual in the pair by a line segment, the recapture image by connecting subsequent sampling locations with line segments, and the sampling image by filling each grid square with the shade matching the number of samples found in that cell. This process is described in more detail in Chapter II.

The final training dataset consisted of 10000 datapoints for each potential log-likelihood ratio cutoff, with one datapoint consisting of a set of images and a population size. The potential log-likelihood ratio cutoffs were 3, 4, 5, and 6.

Training and testing. In the first step of network training and testing, we divided the training dataset into a cross-validation set with 75% of the simulations and a test set with the remaining 25%. The test set was set aside until the final model was chosen and trained.

In the second step, we chose the log-likelihood ratio cutoff for kin estimation using the cross-validation set. For each potential log-likelihood ratio cutoff, the cross-validation set contained 7500 datapoints with a set of images produced under the cutoff and a population size for each datapoint. For each potential cutoff, these datapoints were used to measure mean-squared error in population size predictions through five-fold cross validation. The 7500 datapoints were divided into 5 equal parts, the network was trained on 4/5 of these parts and mean-squared error of predictions measured on the remaining 1/5, and this process was repeated five times. The final mean-squared error was the average over the five parts. At the end of this cross-validation step, we chose the cutoff with the lowest mean-squared error. In the

third step, we trained the final model on all 7500 datapoints in the cross-validation set with the chosen cutoff. Training in both the cross-validation and training steps was for 20 epochs with an Adam optimizer, mean-squared error loss function, and batch size of 10.

In the final step, we evaluated the performance of the model on the test set of simulations. We used the final model to predict population size for each set of images in the test set, then compared predicted size to true size. To measure accuracy of the network, we calculated mean relative absolute error (MRAE) as the mean over all test simulations of $|\text{predicted size} - \text{true size}|\,/\text{true size}$. More accurate estimators have lower MRAE. To measure bias, we calculated mean relative error (MRE) as the mean of $(\text{predicted size} - \text{true size})/\text{true size}$. Less biased estimators have MRE that is closer to zero.

Comparison to capture-recapture. For comparison, we estimated population size for each simulation in the test set using capture-recapture and computed MRAE and MRE over all test simulations. We assumed that recaptures were identified without error, and so the performance of capture-recapture does not depend on the number of sequenced microsatellites. Capture-recapture estimates were obtained using the `capwire` package with the two innate rates model [41].

3.2.4 Estimation of population size in Kibale. To estimate population size of elephants in Kibale, we created images for the empirical dataset using the same process as for the training dataset and using the log-likelihood ratio cutoff for kin estimation chosen in the network training step. We then passed the images through the trained network to get an estimate of population size, $\hat{N}$.

To estimate uncertainty, we used parametric bootstrapping. We simulated 500 elephant datasets with carrying capacity $\hat{N}$, created images from these datasets using

the chosen log-likelihood ratio cutoff, and passed the images through the network to get 500 bootstrap replicates. The 95% confidence interval is then computed from the replicates.

3.3 Results

3.3.1 Parameterizing and validating the individual-based simulation model.

Because our methods use a simulation in place of a model, accurately parameterizing the simulation is important for getting accurate estimates of population size. Social structure and fertility are likely the most important aspects of the model to accurately parameterize. Samples in Kibale are clustered in areas where elephants are found, and so the number of kin pairs in the sample and their distribution across the landscape depends strongly on the sizes of social groups. Female fertility influences variance in reproductive number which influences the probability two individuals are kin.

One option for parameterizing the model would be to infer parameters controlling group size and female fertility directly from the empirical data. However, inferring these parameters would add a large amount of uncertainty, especially for fertility because we do not have ages of sampled individuals. To reduce uncertainty, we used information from previous studies of elephants to fix the parameters.

To determine the values of the parameters controlling social structure and female fertility, we simulated populations with different values of the parameters, measured group size, realized fertility, and realized reproductive value, and chose parameters based on previous studies of savanna and forest elephants.

Social structure. We first explored the effects of the three parameters controlling social group dynamics, α, β, and Γ, on group size. α and β, which scale the probability of merging or splitting, respectively, did not affect average group size

except for extremely large values of α (> 20) or extremely small values of β (< 0.05), so we fixed these parameters at $\alpha = 2$ and $\beta = 1$. Average group size scaled roughly linearly with Γ (Figure A.3), with a small amount of variation between simulation runs.

We chose to fix Γ at 7, which resulted in an average group size of 7.9 total individuals, 3.5 adults, and 4.4 juveniles (Figure A.4). This group size is between the group sizes of savanna elephants and forest elephants. Within a single simulation, group sizes varied quite a bit. For example, in a single simulation with population size 500, total group sizes ranged between 1 and 16, with the number of adults ranging between 1 and 7 and the number of juveniles between 0 and 11 (Figure A.4). These groups had between 0 and 3 juvenile members per adult member.

Fertility. Modeled female fertility is controlled by a single parameter, the maximum probability a female is fertile ($P_{\max}$). We chose this parameter by running simulations for six values of $P_{\max}$: 0.15, 0.2, 0.25, 0.3, 0.35, and 0.4. For each value we ran 100 simulations, with carrying capacity for each simulation drawn from a uniform distribution between 100 and 1500. We then computed simulated fertility (the probability an individual of age a reproduces) and simulated reproductive value (the expected number of future offspring for an individual of age a) for each value of $P_{\max}$, and compare these values to those estimated for populations of savanna and forest elephants. We chose to set $P_{\max} = 0.2$. For $P_{\max} = 0.2$, simulated fertility increases linearly from 0 to around 0.11 for ages 10 to 23, plateaus around 0.11 for ages 24-49, and declines linearly to 0 for ages over 50 (Figure 8). This pattern qualitatively matches the fertility values observed for forest elephants in Dzanga Bai [59], but with a peak fertility value closer to the savanna elephants in Samburu, Kenya [62]. For $P_{\max} = 0.2$, simulated reproductive value is 1.7 for age 0, peaks at 2.3 for

age 14, then declines (Figure 8). These reproductive values are slightly higher than those estimated for Dzanga Bai. In Dzanga Bai, reproductive value was 1.5 at age 0, peaked at 1.75 for age 15, and then declined [59].

The reproductive values calculated from the simulation capture the effects of both age-dependent and density-dependent survival. To isolate the effect of age-dependent survival, we computed theoretical reproductive value at each age based on age-dependent survival values. Theoretical reproductive value is higher than the realized value for ages 0 to 45 (Figure 8), suggesting that in the absence of density-dependence, simulated populations would be increasing in size.

3.3.2 Kin estimation. We first evaluated the effect of the log-likelihood ratio cutoff on specificity and sensitivity of kin estimation using Mendelian inheritance simulations from `CKMRsim` [1]. We ran simulations for both the 14 microsatellites in the empirical dataset and for a hypothetical dataset with 56 microsatellites composed of 4 copies of the original 14 loci.

For 14 microsatellites, kin estimation was very sensitive to the log-likelihood ratio cutoff. For a cutoff of 3, most true parent-offspring pairs were estimated to be parent-offspring (71.4%), with about equal proportions of the remaining pairs estimated to be full- or half-siblings (12.9%) or unrelated (15.6%) (Figure 9). However, even though the percentage of unrelated pairs called as parent-offspring was low at this cutoff (0.6%), because we expect most pair comparisons to be between truly unrelated individuals, specificity is very low. For example, if 100 of the $\binom{124}{2} = 7626$ pairs of individuals were truly related, then we would expect $7526 \cdot 0.006 \approx 45$ pairs to be called as parent-offspring when they are actually unrelated. This means that a large proportion of parent-offspring kin calls would be false positives. Increasing the cutoff greatly increased specificity, but at the cost of also decreasing the number of

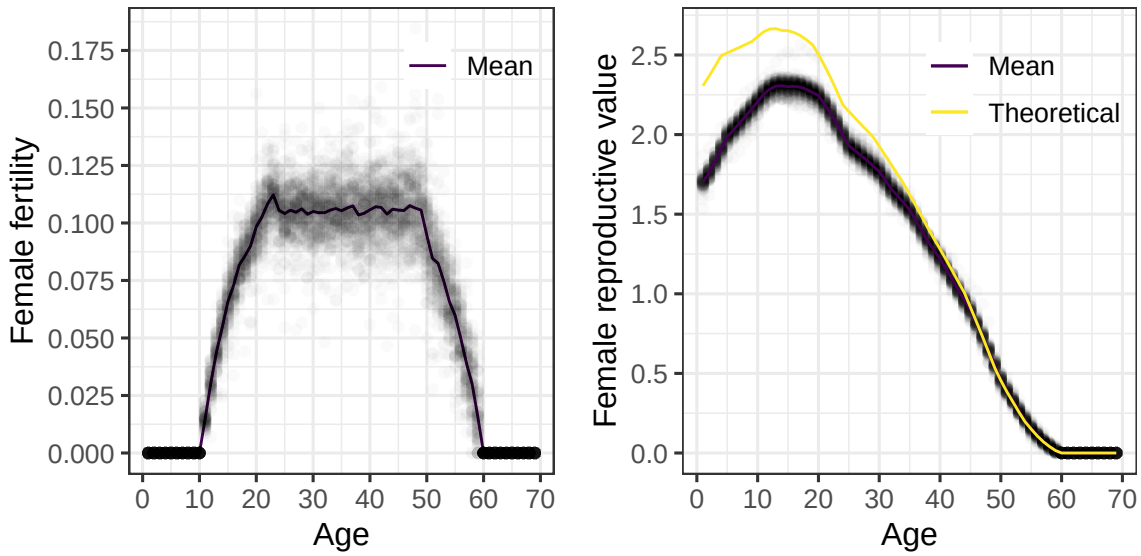

(a) (b)

Figure 8. Fertility **(a)** and reproductive value **(b)** for 100 simulated populations of elephants in Kibale with carrying capacities between 100 and 1500. To compute fertility at age a, we determined the number of females who reached age a in the simulation and computed the proportion of these females who produced an offspring at age a. To compute reproductive value, we found all females who reached age a in the simulation, computed the number of offspring produced by each of these females at or after age a, then took the average. Theoretical reproductive value is based on only age-dependent survival. To compute theoretical reproductive value, we calculated $\sum_{y=a}^{70} (\ell_y/\ell_a)\, m_y$ where ℓ_y is the probability a female survives to age a in the absence of density dependence and m_a is the mean fertility at age a averaged over all simulations.

true parent-offspring pairs identified. At a cutoff of 5.15, only 45.8% of true parent-offspring pairs were identified and most of the remaining pairs were estimated to be unrelated (45.1%). However, only $7526 \cdot 0.0005 \approx 4$ unrelated pairs were expected to be called as parent-offspring at this cutoff. Half- and full- sibling pairs experienced the same tradeoff between sensitivity and specificity but with much lower sensitivity. Only 32.8% of half- or full-siblings were identified with a cutoff of 3 and 19.7% with a cutoff of 5.15 (Figure 9).

For 56 microsatellites, kin estimation had much higher specificity and sensitivity at all log-likelihood ratio cutoffs. Over 95% of parent-offspring pairs were estimated to be parent-offspring at all cutoffs, and all remaining pairs were estimated to be either half- or full- siblings. Over 80% of half- and full-sibling pairs were estimated to be half- or full-siblings at a cutoff of 3, and this percentage decreased to 60% at a cutoff of 7. Almost all of the remaining pairs were estimated to be unrelated. None of the unrelated pairs were called as parent-offspring. The percentage of unrelated pairs called as full- or half- siblings was high at a cutoff of 3 (0.6%) and declined rapidly to 0 at a cutoff of 7 (Figure 9).

We next estimated kin relationships for the $\binom{124}{2} = 7626$ pairs of individuals in the empirical dataset. For a log-likelihood ratio cutoff of 3, the number of estimated pairs was 114 for parent-offspring and 94 for siblings. The number of estimated kin pairs declined sharply as the log-likelihood ratio cutoff increased, with 11 estimated parent-offspring pairs and 5 sibling pairs at a cutoff of 7 (Figure A.6).

3.3.3 Neural network training and testing. We tested the performance of two neural network architectures. The first neural network uses parent-offspring pairs, sibling pairs, recaptures, and sampling intensity to estimate population size and the second network eliminates the recaptures and only uses parent-offspring, siblings,

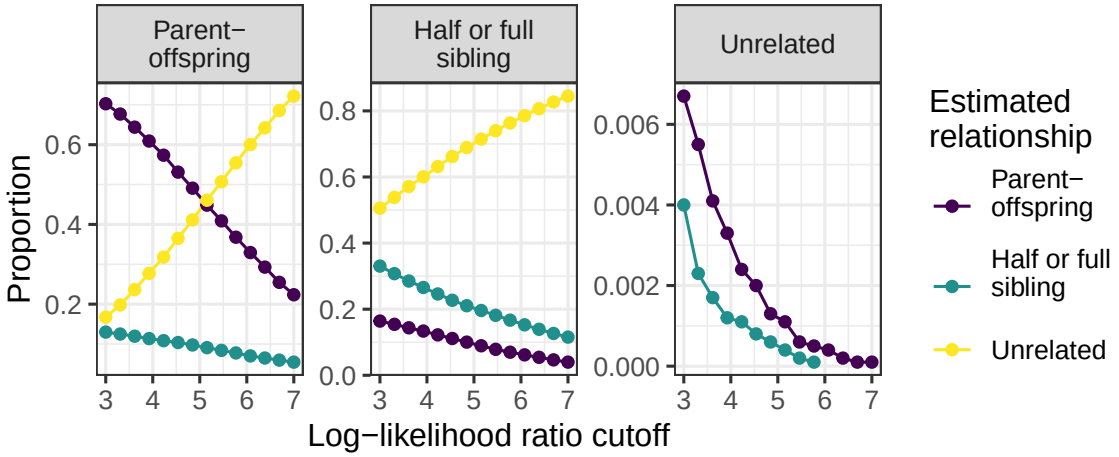

(a) Simulations with 14 microsatellites.

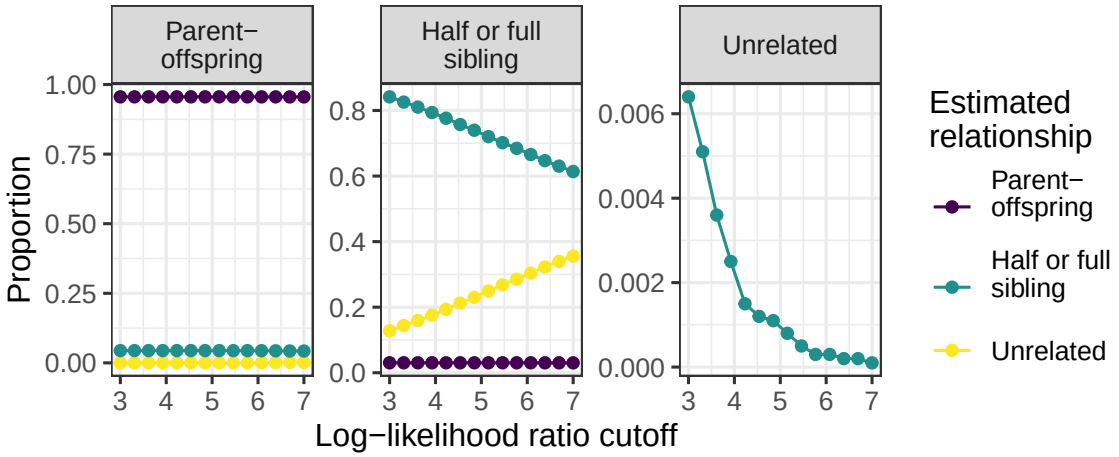

(b) Simulations with 56 microsatellites.

Figure 9. Error rates for estimating kin pairs for **(a)** 14 microsatellites and **(b)** 56 microsatellites. The error rates were computed from 10000 simulations of pairs of genotypes for each of parent-offspring, full-sibling, half-sibling, and unrelated pairs in `CKMRsim` [1]. Full-sibling and half-sibling pairs were then combined. Each plot represents a true relationship and the lines are the proportion of simulated pairs estimated to be each relationship.

and intensity. We chose to test both architectures because they represent different use cases. The Kibale elephant dataset has a significant number of recaptures, and so including these recaptures as input is expected to give the best estimates. However, sampling plans that get recaptures tend to be more time and labor intensive than those that do not, and so testing a network without recaptures measures how well we might be able to estimate population size with a less intensive sampling plan. Testing the network without recaptures also allows us to measure how much information is gained from recaptures.

We used two sets of simulated data to train and test the network, the first with the original number of microsatellites in the empirical dataset (14) and the second with 4 times as many microsatellites (56). The allele frequencies for the 14 microsatellites in the first set of simulations were initialized with the same allele frequencies as the empirical dataset. The initial allele frequencies for the 56 microsatellites in the second set of simulations were composed of 4 copies of the allele frequencies for the empirical dataset.

For the empirical dataset, we expect a large amount of uncertainty in estimates of population size due to the uncertainty in kin pair estimation inherent in using only 14 microsatellite loci. However, if CKMR works well for elephants, then we might design a study with the intention of accurately estimating kin pairs. The second simulated dataset with 56 microsatellites allows us to measure the efficacy of CKMR in this case.

Ideal log likelihood ratio cutoff. For each network and each simulated dataset, we first used cross-validation to determine the best log-likelihood ratio cutoff for kin estimation. The ideal cutoff varied between networks and number of microsatellites (Figure A.5). For 14 microsatellites, for both networks, mean squared

error was lowest for a cutoff of 6. Under this cutoff, we expect to detect about 33% of parent-offspring pairs and 15% of half- or full- sibling pairs, and estimates for the empirical dataset are based on 23 parent-offspring pairs and 9 half- or full-sibling pairs (Figure A.6). For 56 microsatellites, mean squared error was lowest for a cutoff of 4 for the network with recaptures and 5 for the network without recaptures. Under either cutoff we expect to detect about 96% of parent-offspring pairs. We expect to detect 79% of half- or full- sibling pairs under a cutoff of 4 and 72% under a cutoff of 5.

Test set results. With 56 microsatellites, both networks were highly accurate and had very low bias (Figure 10, Table 5). Mean relative absolute error was 0.246 with recaptures and 0.265 without, and mean relative error was close to 0 for both networks. With 14 microsatellites, the network without recaptures was not very accurate, with a mean relative absolute error of 0.503, and had high positive bias, with a mean relative error of 0.212. Adding recaptures greatly improved the performance of the network, with mean relative absolute error decreasing by almost 30% to 0.361 and positive bias decreasing by about 25% to 0.160.

The main difference between the networks in this chapter and in Chapter II is uncertainty in kin estimation. In Chapter II, we assumed that kin pairs were known without error and the trained network with recaptures was over 50% more accurate, with mean relative error of about 0.12 (Figure 5).

Comparison to capture-recapture. For comparison, we estimated population size using capture-recapture for the same test simulations as for the networks. Capture-recapture estimates were obtained using the two innate rates model in `capwire` [41] and assuming recaptures were known without error. Capture-recapture performed very well for simulated populations with sizes below 400, but as

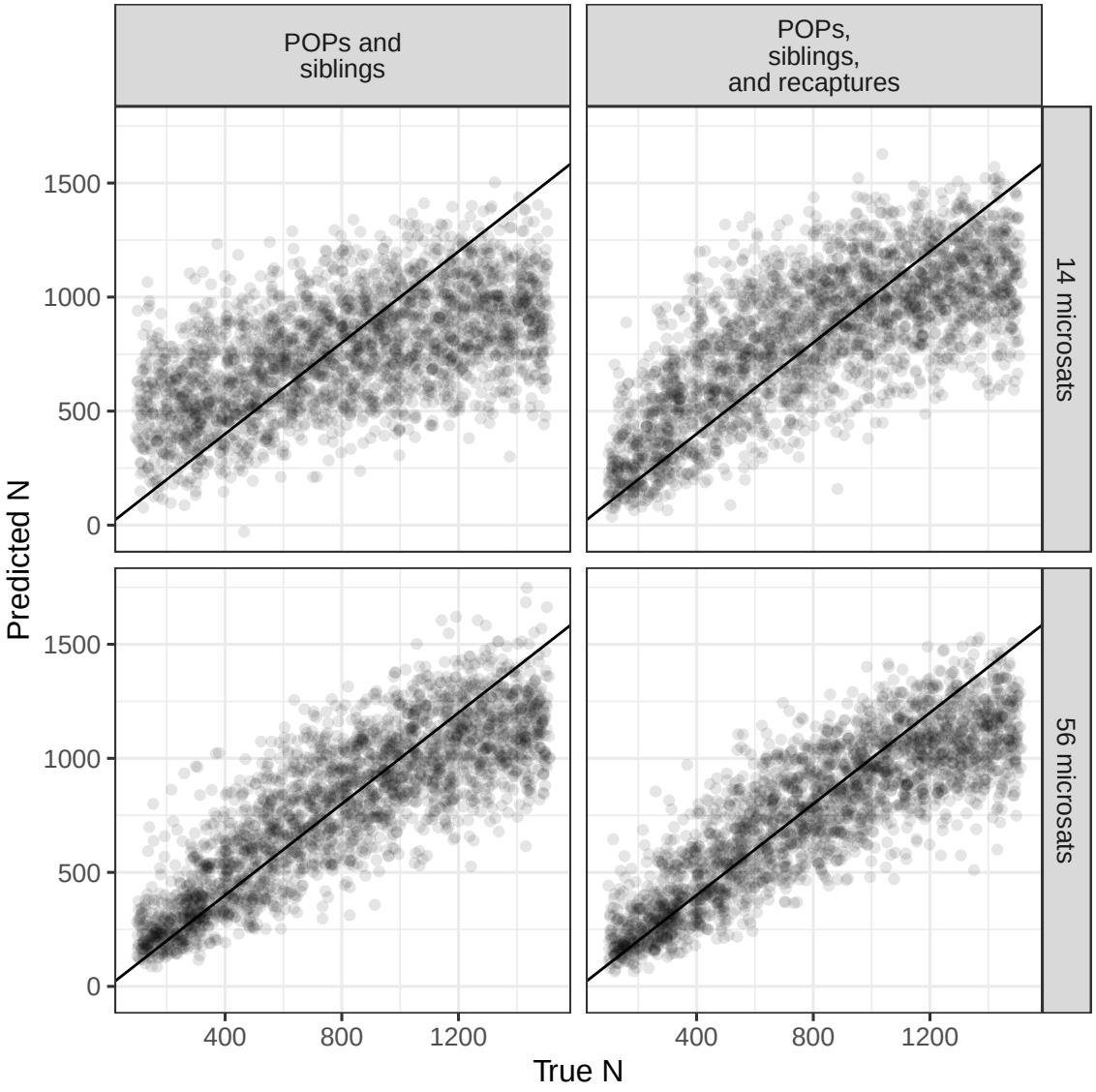

Figure 10. True vs. predicted population size for a held out test set of simulations for two simulated datasets (rows) and two networks (columns). The first dataset is simulations with 14 microsatellites and the second is a hypothetical dataset with 56 microsatellites composed of 4 copies of the original 14. One network takes as input parent-offspring pairs (POPs) and full- and half-sibling pairs (siblings) and the other network takes as input POPs, siblings, and recaptures.

Method	Number of microsatellites	Mean relative absolute error (MRAE)	Mean relative error (MRE)
Network with POPs and siblings	14	0.503	0.212
Network with POPs, siblings, and recaptures	14	0.361	0.160
Network with POPs and siblings	56	0.265	0.075
Network with POPs, siblings, and recaptures	56	0.246	0.024
`capwire` with recaptures		0.413	0.322

Table 5. Performance of networks and capture-recapture on simulated elephant populations. The original dataset has 14 microsatellites. The hypothetical dataset with 56 microsatellites is composed of 4 copies of the original 14 microsatellites. One network takes as input parent-offspring pairs (POPs) and full- and half-sibling pairs (siblings) and the other network takes as input POPs, siblings, and recaptures. Capture-recapture estimates were obtained using the program `capwire` and the two innate rates model [41]. Recaptures were assumed to be known without error, and so the number of simulated microsatellites does not influence performance of the estimator. Relative absolute error is calculated as $|\text{predicted} - \text{true}| / \text{true}$ and relative error as $(\text{predicted} - \text{true}) / \text{true}$.

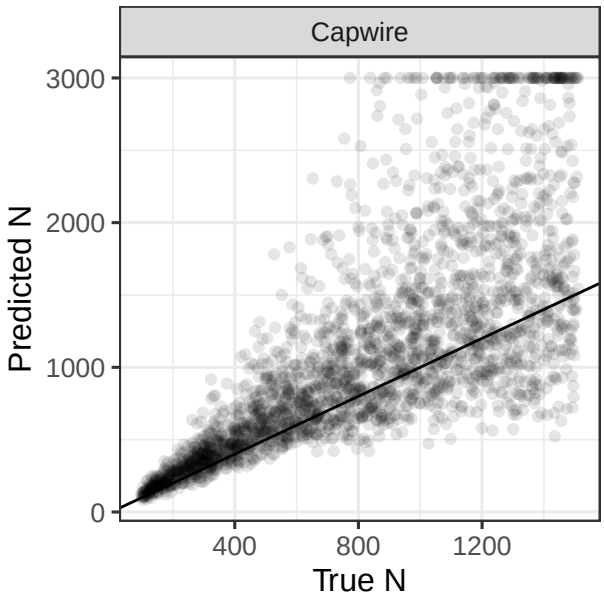

Figure 11. Performance of capture-recapture on a simulated dataset. Estimates were obtained using the program `capwire` with the two innate rates model [41]. Recaptures were assumed to be known without error, and so the number of simulated microsatellites does not influence performance of the estimator.

true population size increased, estimates of population size were often much higher than the true size (Figure 11). Over all test simulations, capture-recapture had fairly low accuracy, with a mean relative absolute error of 0.413, and high positive bias, with a mean relative error of 0.322 (Table 5).

Three of the four combinations of network and dataset performed better than capture-recapture. For 14 microsatellites, the network with parent-offspring pairs, siblings, and recaptures had slightly lower mean relative absolute error than capture-recapture, but had much lower positive bias. For 56 microsatellites, networks both with and without recaptures had much lower mean relative absolute error than capture-recapture and were approximately unbiased.

3.3.4 Estimation of population size in Kibale. To estimate population size for the empirical dataset, we used the network with recaptures, parent-offspring

pairs, and half- and full-sibling pairs. We then computed a 95% confidence interval from 500 parametric bootstrap replicates (Figure A.7). We estimated that population size in Kibale is 684 with a 95% confidence interval of 389 to 1255.

3.4 Discussion

In this chapter, we extended the simulation-based close-kin mark-recapture methods developed in Chapter II to account for two common situations in populations of conservation concern: social structure with groups of related individuals traveling together and high uncertainty in kin estimation due to very few sequenced loci. We then tested the feasibility of using our methods for genetic population monitoring of elephants in Kibale National Park. We found that with 14 microsatellite loci, kin estimation was highly uncertainty and contributed to high uncertainty in CKMR estimates. However, our CKMR network with recaptures still performed better than capture-recapture, with 12.5% lower mean relative absolute error and 50% lower relative bias. With a greater number of sequenced microsatellites (56), kin estimation had very low uncertainty and our network performed incredibly well, even when recaptures were not included, with mean relative absolute errors of 0.265 and 0.246 for with recaptures and without recaptures, respectively. Population size estimates were approximately unbiased both with and without recaptures. Using our CKMR network with the 14 microsatellite loci available from existing dung samples and including recaptures, we estimated that elephant population size in Kibale is 684 with a 95% confidence interval of 389 to 1255.

We anticipate that our simulation-based CKMR method will be most useful as an alternative to capture-recapture rather than as an alternative to existing CKMR methods. Our CKMR method is the first to our knowledge to model recaptures along with kin pairs, and including recaptures allows our method to be used even when

only small numbers of loci are sequenced and kin estimation is highly uncertain. For elephants, we show that our method leads to more accurate estimates of population size than capture-recapture for an existing dataset with 14 microsatellite loci, and that sequencing more loci from non-invasive samples can lead to even more accurate estimates. Obtaining more sequenced loci from dung samples is possible, but challenging. For example, using DNA preservation cards, de Flamingh et al. [18] were able to obtain low-coverage whole genome sequences from savanna elephant dung piles that were up to 72 hours old. For populations where increased accuracy in estimates of population size is very important or where obtaining genetic samples is very expensive, sequencing more loci from each sample may be a cost-effective strategy for monitoring.

Our estimate of population size in Kibale of 684 with a 95% confidence interval of 389 to 1255 is notably higher than previous estimates, although confidence intervals for all estimates overlap. In 2021, Daniel, Edward and Kennedy [17] estimated population size to be 566 with a 95% CI of 377 to 850 based on a cut transect survey. In 2025, Goodfellow et al. [25] estimated population size to be 573 with a 95% CI of 410 to 916 based on genetic capture-recapture. One source of discrepancy could be immigration. Kibale is connected to Queen Elizabeth National Park in Uganda by the Dura corridor, a protected area designated for elephant movement. Elephants are known to be able to use this corridor [17]; however, migration rates between the parks are unknown. Queen Elizabeth also shares a boundary with Virunga National Park in the Democratic Republic of the Congo, and elephants are known to move between the two parks [35]. One way to account for the impact of immigration from Queen Elizabeth on CKMR estimates would be to add migration between Kibale, Queen Elizabeth, and potentially Virunga to the simulation.

Our estimate also has a larger confidence interval than previous estimates; however, because confidence intervals for the three methods were obtained using different models with different assumptions, the confidence intervals are not comparable. The confidence intervals for our CKMR estimate are likely larger than those for capture-recapture because they are obtained using our simulation model, which incorporates more spatial and social complexity than the multinomial model used for capture-recapture.

The methods we developed in this chapter advance CKMR methods for all species. Many mammals of conservation concern, such as wolves and primates, have complex social structures similar to elephants that make implementing kin-based methods challenging. Wildlife managers already routinely collect non-invasive genetic data for capture-recapture studies, and using our methods can help these managers get better estimates without collecting more samples.

Simulation-based methods for CKMR are just starting to be developed and are very promising; however, accounting for uncertainty in kin estimation is a gap in the two existing methods, Conn [14] and Chapter II. In our method, we fill this gap by accounting for kin uncertainty in the simulation pipeline. This allows us to account for all sources of error in kin estimation. For example, half-sibling, grandparent-grandchild, and aunt-niece relationships all have a relatedness coefficient of 0.25, making them very hard to distinguish without age or recombination information. For populations with long generation times and mate fidelity, likelihood-based models must be adapted to include the possibility that estimated half-sibling pairs also include these other relationships with the same coefficient of relatedness [14]. By incorporating the kin estimation step into our simulation pipeline, we automatically account for all sources of error, including confounding of kin relationships.

Although simulation-based methods are very promising for CKMR, they still have several limitations. Some of these limitations are specific to simulation-based methods and can be overcome with future methods development. For example, we assume that survival and fecundity at age are known without error, which is likely unrealistic. Likelihood-based CKMR studies often estimate these parameters from the observed data and so make fewer assumptions. For example, in their CKMR study of southern bluefin tuna, Bravington, Grewe and Davies [11] estimated adult survival, relationship between age, body mass, and female fecundity, and abundance from parent-offspring pairs and from data on length, sex, and ages of females. Our simulation-based methods could be adapted to perform similar analyses. For example, to simultaneously output survival and abundance, we could modify the neural network architecture to take as input ages of sampled individuals and to output both survival parameters and abundance.

Another limitation is fundamental to all close-kin methods. Because the number of close-kin pairs is influenced by both census size and variance in number of offspring between individuals, for some situations population size might not be identifiable without prior information on variance in offspring number. For example, the number of half-sibling pairs cannot distinguish between a population of 100 parents, 50 of whom reproduced, and a population of 50 parents, all of whom reproduced. Without prior information, close-kin methods can still be used to estimate effective population size, as described in Waples and Feutry [61] and Babyn et al. [4].

Simulation-based close-kin mark-recapture methods have the potential to accurately model many of the complex dynamics of species of conservation concern. In this chapter, we make a valuable contribution to these methods by accounting for social groups and high uncertainty in kin estimation.

CHAPTER IV

CONCLUSION

Monitoring the size of wildlife populations is critical for conserving species and sustainably managing harvested populations, but population size is often challenging and labor intensive to estimate. In my dissertation, I improved methods for estimating population size from genetic data. I focused on a class of methods called close-kin mark-recapture (CKMR) that estimate population size from close-kin pairs, such as parents and offspring and half-siblings. CKMR is very promising, but a limitation of current, likelihood-based methods is that they do not model the complex spatial and social dynamics that are important in many species of conservation concern. In my dissertation, I overcame this limitation by developing, testing, and applying a spatially explicit CKMR method using simulation-based inference and neural networks.

In Chapter II, I developed and tested a spatially explicit CKMR method. The method, called CKMRnn, is a convolutional neural network (CNN) that takes as input images representing maps of kin pairs, sampling intensity, and, optionally, recaptures, and outputs a single population size. The network is trained on individual-based, spatially explicit simulations implemented in the population genetic simulation program SLiM [29]. I first tested the method on simulated populations and found that CKMRnn was unbiased, even with limited dispersal and high spatial bias in sampling, a situation in which non-spatial methods are biased. CKMRnn was highly accurate and estimated population size to within 6% of the true value. When population trend was unknown, estimates were still unbiased but had slightly higher error, with estimates within about 10% of the true value. I next tested CKMRnn on a population of elephants in Kibale National Park using genetic data collected by Goodfellow et al. [25]. When parent-offspring pairs were assumed to be known without error, estimated

population size agreed with previous estimates but with a 32% smaller confidence interval.

The population size estimated for elephants in Chapter II does not accurately represent two important sources of uncertainty: uncertainty in estimating kin pairs from low quality genetic data and complex social structure with related individuals traveling together. In Chapter III, I extended the method to model these two sources. I developed and parameterized a spatially explicit, individual-based simulation of elephants that models matrilineal social structure and inheritance of microsatellites, estimated kin pairs from the simulated microsatellites, and trained the network on estimated kin pairs. For the 14 microsatellites sequenced in Kibale, error in kin estimation was high and contributed to high uncertainty in estimates of population size when recaptures were not included as input to the network. When recaptures were included, the network performed much better and was slightly more accurate than capture-recapture. For a hypothetical dataset with 56 microsatellites composed of four copies of the original 14 microsatellites, error in kin estimation was much lower and estimates of population size were very accurate. Mean relative absolute error was around 0.27 even without including recaptures. Chapter III demonstrates that CKMR could significantly improve estimates of population size for elephants in Kibale, especially with more sequenced loci.

The methods I developed are very effective for estimating a single population size, an important first step for spatially explicit CKMR. However, fully realizing the potential of CKMR methods will require developing methods to estimate population density across the landscape. Estimating population density is important for two reasons: first, in populations without clear boundaries, population density is a more meaningful quantity than a single population size, and second, in populations where

density varies across the landscape, a map of population density is more useful than a single number. Spatially explicit capture-recapture methods that estimate density across the landscape are already widely used and have been extended to estimate ecological parameters such as the relationship between habitat and population density [20, 47, 48]. Spatially explicit capture-recapture models each individual as having an activity center with activity centers distributed as a point process over the landscape, and then models the probability of capture of a specific individual at a trapping location as a function of the distance from its activity center to the trapping location [20]. It would be possible to model close-kin mark-recapture in the same way, but the probability of capturing a kin pair depends on fertility and survival as well as distance, so the models would quickly become complex. The simulation-based framework from my dissertation is a potential solution. The methods I developed could be adapted to estimate population density rather than size or to output a map of population density across the landscape.

Many species live and move on large continuous landscapes and interact with each other in complex social systems. These species are often threatened by human activities such as poaching and habitat loss. The methods I developed in my dissertation make a valuable contribution to genetic monitoring of these species and demonstrate the power of spatially explicit simulation-based inference for conservation biology. The earth will continue to face an extinction crisis for many generations and methods like mine can help minimize effects on species we love.

APPENDIX

APPENDIX A

A.1 Additional figures for Chapter II

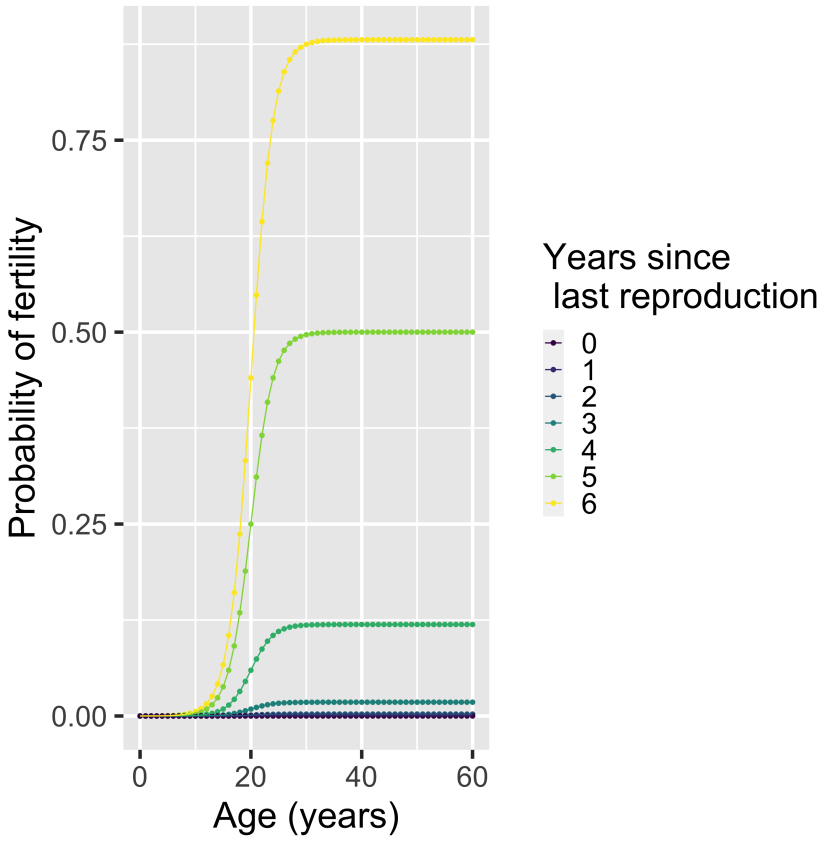

Figure A.1. Female fertility for the elephant simulation in Chapter II. The plot shows the probability that a simulated female elephant is fertile in a given year, given her age and the number of years since she last reproduced.

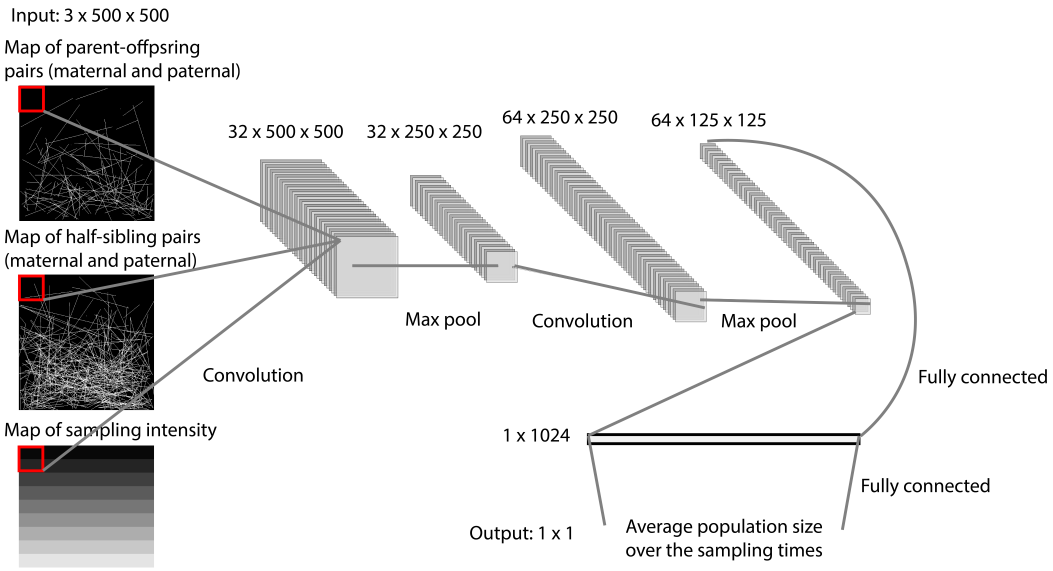

Figure A.2. Convolutional neural network architecture for the network in Chapter II, CKMRnn.

A.2 Additional figures for Chapter III

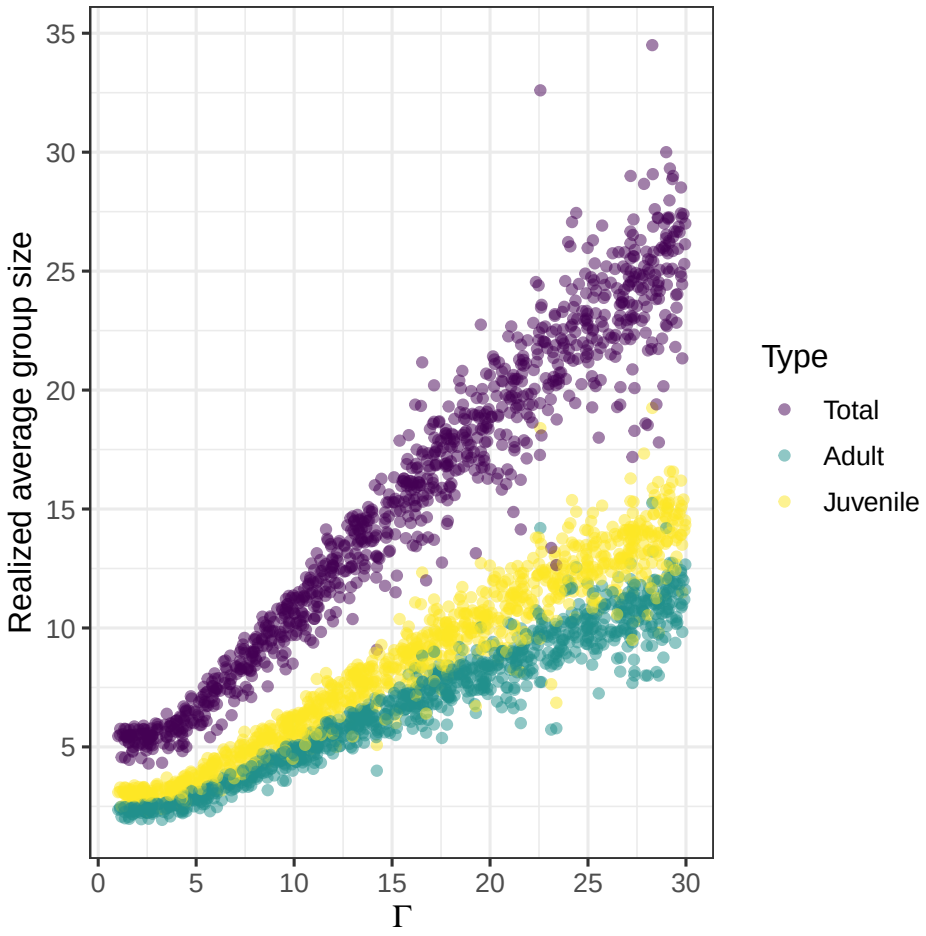

Figure A.3. For the elephant simulations in Chapter III, relationship between the group size parameter Γ and realized average group size across 1000 simulations with population sizes varying between 100 and 1500.

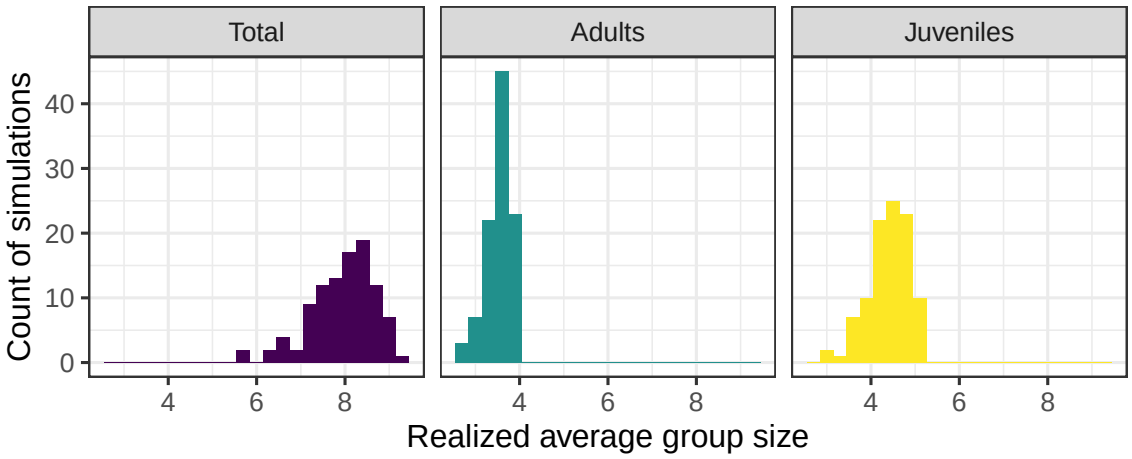

(a) Distribution of average final group sizes across 1000 simulation runs.

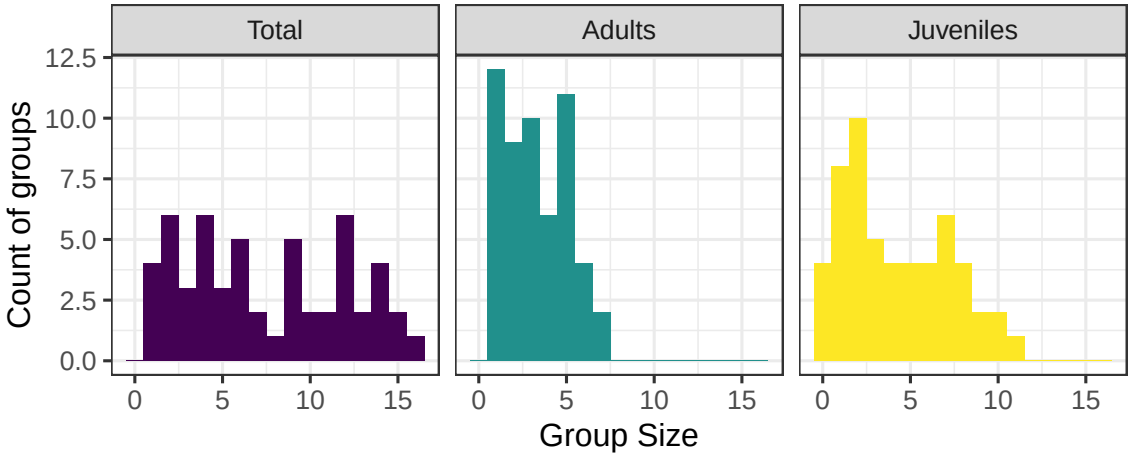

(b) Distribution of group sizes for a single simulation run.

Figure A.4. For the elephant simulations in Chapter III, variation in group size between and within elephant simulations with carrying capacity between 100 and 1500 **(a)** and within a single simulation with carrying capacity 500 **(b)**. For all simulations the group size parameter was set to $\Gamma = 7$. Group sizes were calculated in the final year (200) of the simulation. **(a)** is based on 1000 simulations and **(b)** is based on a single simulation.

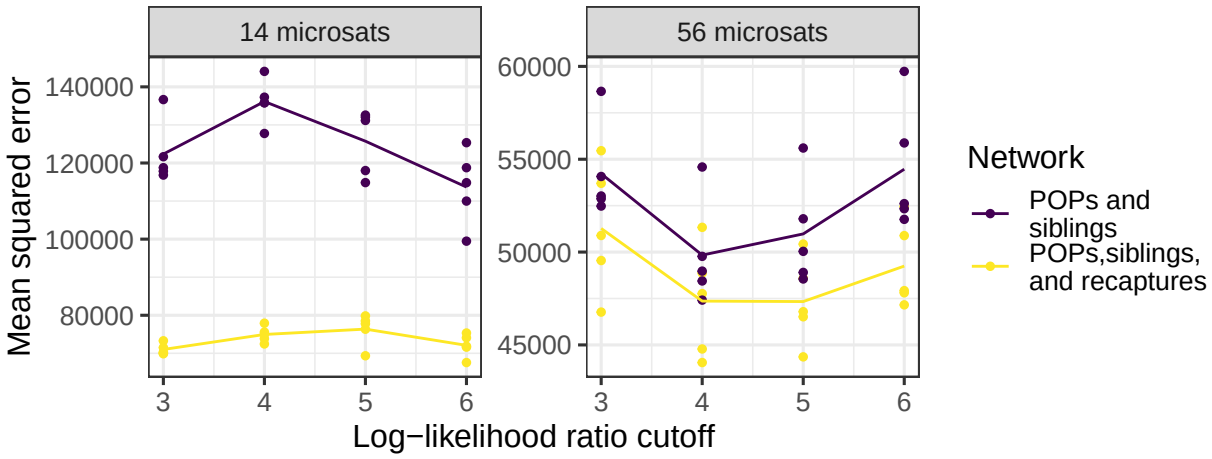

Figure A.5. Cross validation results for choosing the ideal log-likelihood ratio cutoff for estimating kin for each dataset and each network. The two datasets are 14 simulated microsatellites and 56 simulated microsatellites. One network takes as input parent-offspring pairs (POPs) and full- and half-sibling pairs (siblings) and the other network takes as input POPs, siblings, and recaptures. The mean squared error for predicting population size for each cutoff was calculated through 5-fold cross validation. Each point is the mean squared error for a single fold and the line is the average across all folds.

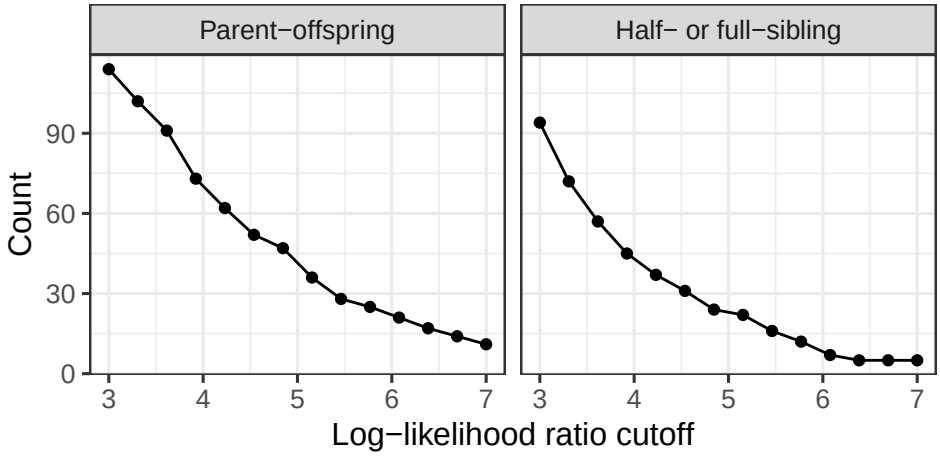

Figure A.6. Counts of estimated kin pairs for the 124 unique elephants sampled in Kibale National Park.

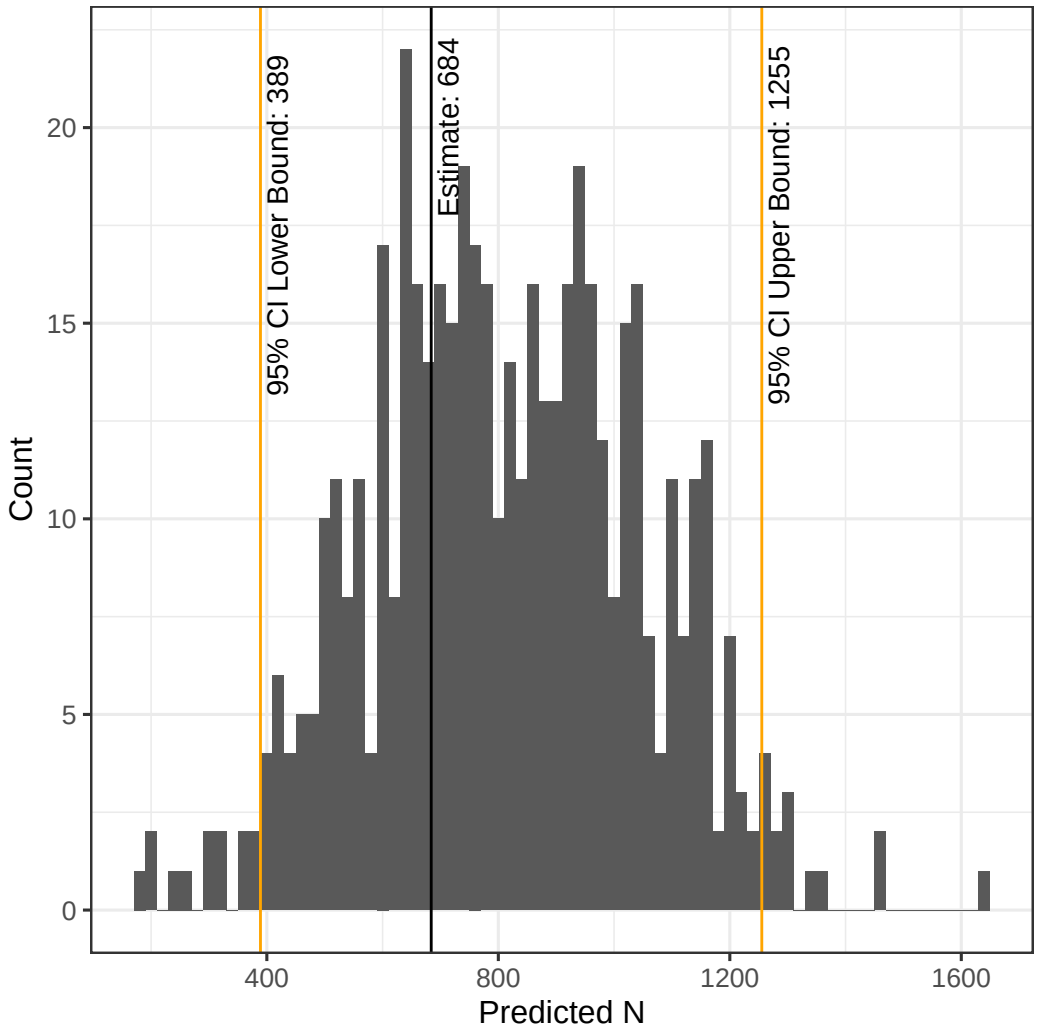

Figure A.7. Bootstrap distribution for empirical population size estimate of African elephants in Kibale National Park. Estimate was based on parent-offspring pairs, half- and full-sibling pairs, and recaptures.

Bibliography

[1] Eric C. Anderson. *CKMRsim: Inference of Pairwise Relationships Using Likelihood Ratios*. manual. 2024.

[2] Peter Armbruster and Russell Lande. "A Population Viability Analysis for African Elephant (Loxodonta Africana): How Big Should Reserves Be?" In: *Conservation Biology* 7.3 (1993), pp. 602–610. ISSN: 0888-8892. JSTOR: 2386689.

[3] T. K. Athira and T. N. C. Vidya. "Elephant Social Systems: What Do We Know and How Have Molecular Tools Helped?" In: *Journal of the Indian Institute of Science* 101.2 (1st Apr. 2021), pp. 257–278. ISSN: 0019-4964. DOI: 10.1007/s41745-021-00226-4.

[4] Jonathan Babyn et al. "Estimating Effective Population Size Using Close-Kin Mark–Recapture". In: *Methods in Ecology and Evolution* 15.11 (2024), pp. 2059–2073. ISSN: 2041-210X. DOI: 10.1111/2041-210X.14419.

[5] Sophie Baillargeon and Louis-Paul Rivest. "Rcapture: Loglinear Models for Capture-Recapture in R". In: *Journal of Statistical Software* ().

[6] Mark A. Beaumont. "Approximate Bayesian Computation in Evolution and Ecology". In: *Annual Review of Ecology, Evolution, and Systematics* 41.1 (1st Dec. 2010), pp. 379–406. ISSN: 1543-592X, 1545-2069. DOI: 10.1146/annurev-ecolsys-102209-144621.

[7] Christopher Beirne. "African Forest Elephant Movements Depend on Time Scale and Individual Behavior". In: *Scientific Reports* (2021).

[8] Stephen Blake et al. “Roadless Wilderness Area Determines Forest Elephant Movements in the Congo Basin”. In: *PLoS ONE* 3.10 (28th Oct. 2008). Ed. by Craig R. McClain, e3546. ISSN: 1932-6203. DOI: 10.1371/journal.pone.0003546.

[9] John Boulanger, Scott E. Nielsen and Gordon B. Stenhouse. “Using Spatial Mark-Recapture for Conservation Monitoring of Grizzly Bear Populations in Alberta”. In: *Scientific Reports* 8.1 (1 26th Mar. 2018), p. 5204. ISSN: 2045-2322. DOI: 10.1038/s41598-018-23502-3.

[10] Gideon S. Bradburd and Peter L. Ralph. “Spatial Population Genetics: It’s About Time”. In: *Annual Review of Ecology, Evolution, and Systematics* 50.1 (2019), pp. 427–449. DOI: 10.1146/annurev-ecolsys-110316-022659.

[11] Mark V. Bravington, Peter M. Grewe and Campbell R. Davies. “Absolute Abundance of Southern Bluefin Tuna Estimated by Close-Kin Mark-Recapture”. In: *Nature Communications* 7.1 (1 14th Nov. 2016), p. 13162. ISSN: 2041-1723. DOI: 10.1038/ncomms13162.

[12] Mark V. Bravington, Hans J. Skaug and Eric C. Anderson. “Close-Kin Mark-Recapture”. In: *Statistical Science* 31.2 (May 2016), pp. 259–274. ISSN: 0883-4237, 2168-8745. DOI: 10.1214/16-STS552.

[13] Elizabeth T. Chevy et al. “Population Genetics Meets Ecology: A Guide to Individual-Based Simulations in Continuous Landscapes”. In: *Ecology and Evolution* 15.4 (2025), e71098. ISSN: 2045-7758. DOI: 10.1002/ece3.71098.

[14] Paul B. Conn. *Simulation-Based Inference for Close-Kin Mark-Recapture: Implications for Small Populations and Nonrandom Mating*. 20th Dec. 2024.

DOI: 10.1101/2024.12.16.628779. URL: http://biorxiv.org/lookup/doi/10.1101/2024.12.16.628779 (visited on 13/02/2025). Pre-published.

[15] Paul B. Conn et al. "Robustness of Close-Kin Mark–Recapture Estimators to Dispersal Limitation and Spatially Varying Sampling Probabilities". In: *Ecology and Evolution* 10.12 (2020), pp. 5558–5569. ISSN: 2045-7758. DOI: 10.1002/ece3.6296.

[16] Kyle Cranmer, Johann Brehmer and Gilles Louppe. "The Frontier of Simulation-Based Inference". In: *Proceedings of the National Academy of Sciences* 117.48 (Dec. 2020), pp. 30055–30062. ISSN: 0027-8424, 1091-6490. DOI: 10.1073/pnas.1912789117.

[17] Aleper Daniel, Andama Edward and Adriko Kennedy. "Elephant Population Status, Distribution and Conservation Threats in Kibale National Park, Uganda". In: *East African Journal of Environment and Natural Resources* 4.1 (1 8th Dec. 2021), pp. 68–78. ISSN: 2707-4242. DOI: 10.37284/eajenr.4.1.499.

[18] Alida de Flamingh et al. "Combining Methods for Non-Invasive Fecal DNA Enables Whole Genome and Metagenomic Analyses in Wildlife Biology". In: *Frontiers in Genetics* 13 (12th Jan. 2023). ISSN: 1664-8021. DOI: 10.3389/fgene.2022.1021004.

[19] Cornelia Ebert et al. "Estimating Red Deer (Cervus Elaphus) Population Size Based on Non-Invasive Genetic Sampling". In: *European Journal of Wildlife Research* 67.2 (9th Mar. 2021), p. 27. ISSN: 1439-0574. DOI: 10.1007/s10344-021-01456-8.

[20] Murray Efford. "Density Estimation in Live-Trapping Studies". In: *Oikos* 106.3 (2004), pp. 598–610. ISSN: 1600-0706. DOI: 10.1111/j.0030-1299.2004.13043.x.

[21] Murray G. Efford. "Estimation of Population Density by Spatially Explicit Capture–Recapture Analysis of Data from Area Searches". In: *Ecology* 92.12 (2011), pp. 2202–2207. ISSN: 1939-9170. DOI: 10.1890/11-0332.1.

[22] R. A. Fisher. *The Genetical Theory of Natural Selection*. The Genetical Theory of Natural Selection. Oxford, England: Clarendon Press, 1930, pp. xiv, 272. xiv, 272. DOI: 10.5962/bhl.title.27468.

[23] Lex Flagel, Yaniv Brandvain and Daniel R Schrider. "The Unreasonable Effectiveness of Convolutional Neural Networks in Population Genetic Inference". In: *Molecular Biology and Evolution* 36.2 (1st Feb. 2019), pp. 220–238. ISSN: 0737-4038. DOI: 10.1093/molbev/msy224.

[24] Matthew Fuirst et al. "A Review of Aerial Survey Density Estimates of Bearded Seals (Erignathus Barbatus) in the Canadian Arctic Highlights Important Knowledge Gaps and Research Needs". In: *Polar Biology* 46.12 (Dec. 2023), pp. 1251–1263. ISSN: 0722-4060, 1432-2056. DOI: 10.1007/s00300-023-03200-1.

[25] Claire K. Goodfellow et al. *Elephants Inhabiting Two Forested Sites in Western Uganda Exhibit Contrasting Patterns of Species Identity, Density, and History of Hybridization*. 17th May 2025. DOI: 10.1101/2025.05.13.653790. URL: https://www.biorxiv.org/content/10.1101/2025.05.13.653790v1 (visited on 22/05/2025). Pre-published.

[26] Claire Katherine Goodfellow. "Genetic Insights into the Dynamics of Hybridization Between African Elephant Species". PhD thesis. United States – Oregon: University of Oregon, 2023. 140 pp. ISBN: 9798381143874.

[27] David S. Green et al. "Mixed-Severity Wildfire and Salvage Logging Affect the Populations of a Forest-Dependent Carnivoran and a Competitor". In: *Ecosphere* 13.1 (2022), e03877. ISSN: 2150-8925. DOI: 10.1002/ecs2.3877.

[28] Shay Gueron and Simon A. Levin. "The Dynamics of Group Formation". In: *Mathematical Biosciences* 128.1 (1st July 1995), pp. 243–264. ISSN: 0025-5564. DOI: 10.1016/0025-5564(94)00074-A.

[29] Benjamin C. Haller and Philipp W. Messer. "SLiM 4: Multispecies Eco-Evolutionary Modeling". In: *The American Naturalist* 201.5 (1st May 2023), E127–E139. ISSN: 0003-0147, 1537-5323. DOI: 10.1086/723601.

[30] R. M. Hillary et al. "Genetic Relatedness Reveals Total Population Size of White Sharks in Eastern Australia and New Zealand". In: *Scientific Reports* 8.1 (1 8th Feb. 2018), p. 2661. ISSN: 2045-2322. DOI: 10.1038/s41598-018-20593-w.

[31] Richard Huggins. "A Note on the Difficulties Associated with the Analysis of Capture–Recapture Experiments with Heterogeneous Capture Probabilities". In: *Statistics & Probability Letters* 54.2 (15th Sept. 2001), pp. 147–152. ISSN: 0167-7152. DOI: 10.1016/S0167-7152(00)00233-9.

[32] Hans Julius Skaug. "Allele-Sharing Methods for Estimation of Population Size". In: *Biometrics* 57.3 (2001), pp. 750–756. ISSN: 1541-0420. DOI: 10.1111/j.0006-341X.2001.00750.x.

[33] Steven T. Kalinowski, Aaron P. Wagner and Mark L. Taper. "Ml-Relate: A Computer Program for Maximum Likelihood Estimation of Relatedness and Relationship". In: *Molecular Ecology Notes* 6.2 (2006), pp. 576–579. ISSN: 1471-8286. DOI: 10.1111/j.1471-8286.2006.01256.x.

[34] Marty Kardos. "Conservation Genetics". In: *Current Biology* 31.19 (Oct. 2021), R1185–R1190. ISSN: 09609822. DOI: 10.1016/j.cub.2021.08.047.

[35] Michael Keigwin et al. "Impacts on Transboundary Elephant Movements between Queen Elizabeth Conservation Area, Uganda and Parc National Des Virunga, Democratic Republic of Congo". In: *Pachyderm* 57 (21st July 2016), pp. 118–121. ISSN: 1026-2881.

[36] William A. Link. "Nonidentifiability of Population Size from Capture-Recapture Data with Heterogeneous Detection Probabilities". In: *Biometrics* 59.4 (1st Dec. 2003), pp. 1123–1130. ISSN: 0006-341X. DOI: 10.1111/j.0006-341X.2003.00129.x.

[37] Luke R. Lloyd-Jones et al. "Close-Kin Mark-Recapture Informs Critically Endangered Terrestrial Mammal Status". In: *Scientific Reports* 13.1 (1 2nd Aug. 2023), p. 12512. ISSN: 2045-2322. DOI: 10.1038/s41598-023-38639-z.

[38] Paul M. Lukacs and Kenneth P. Burnham. "Review of Capture–Recapture Methods Applicable to Noninvasive Genetic Sampling". In: *Molecular Ecology* 14.13 (2005), pp. 3909–3919. ISSN: 1365-294X. DOI: 10.1111/j.1365-294X.2005.02717.x.

[39] Robert Malpas. "Elephant Losses in Uganda – and Some Gains". In: *Oryx* 16.1 (May 1981), pp. 41–44. ISSN: 1365-3008, 0030-6053. DOI: 10.1017/S0030605300016720.

[40] Brandon D. Merriell, Micheline Manseau and Paul J. Wilson. "Assessing the Suitability of a One-Time Sampling Event for Close-Kin Mark-Recapture: A Caribou Case Study". In: *Ecology and Evolution* 14.9 (2024), e70230. ISSN: 2045-7758. DOI: 10.1002/ece3.70230.

[41] Craig R. Miller, Paul Joyce and Lisette P. Waits. "A New Method for Estimating the Size of Small Populations from Genetic Mark–Recapture Data". In: *Molecular Ecology* 14.7 (2005), pp. 1991–2005. ISSN: 1365-294X. DOI: 10.1111/j.1365-294X.2005.02577.x.

[42] David Mitchell. "Uganda's Elephants Near Extinction?" In: *Environmental Conservation* 7.3 (Oct. 1980), pp. 212–212. ISSN: 1469-4387, 0376-8929. DOI: 10.1017/S0376892900007608.

[43] Toby A. Patterson et al. "Rapid Assessment of Adult Abundance and Demographic Connectivity from Juvenile Kin Pairs in a Critically Endangered Species". In: *Science Advances* 8.51 (21st Dec. 2022), eadd1679. DOI: 10.1126/sciadv.add1679.

[44] Matthew W. Pennell et al. "Capwire: A R Package for Estimating Population Census Size from Non-Invasive Genetic Sampling". In: *Molecular Ecology Resources* 13.1 (2013), pp. 154–157. ISSN: 1755-0998. DOI: 10.1111/1755-0998.12019.

[45] Felix T. Petersma et al. "Age Is Not Just a Number: How Incorrect Ageing Impacts Close-Kin Mark-Recapture Estimates of Population Size".

In: *Ecology and Evolution* 14.6 (2024), e11352. ISSN: 2045-7758. DOI: 10.1002/ece3.11352.

[46] Louis-Paul Rivest and Sophie Baillargeon. "Applications and Extensions of Chao's Moment Estimator for the Size of a Closed Population". In: *Biometrics* 63.4 (2007), pp. 999–1006. ISSN: 1541-0420. DOI: 10.1111/j.1541-0420.2007.00779.x.

[47] J. Andrew Royle, Angela K. Fuller and Christopher Sutherland. "Unifying Population and Landscape Ecology with Spatial Capture–Recapture". In: *Ecography* 41.3 (2018), pp. 444–456. ISSN: 1600-0587. DOI: 10.1111/ecog.03170.

[48] J. Andrew Royle et al. *Spatial Capture-Recapture*. San Diego, UNITED STATES: Elsevier Science & Technology, 2013. ISBN: 978-0-12-407152-0.

[49] Daniel E. Ruzzante et al. "Validation of Close-Kin Mark–Recapture (CKMR) Methods for Estimating Population Abundance". In: *Methods in Ecology and Evolution* 10.9 (2019), pp. 1445–1453. ISSN: 2041-210X. DOI: 10.1111/2041-210X.13243.

[50] Anthony Sévêque et al. "Sources of Bias in Applying Close-Kin Mark–Recapture to Terrestrial Game Species with Different Life Histories". In: *Ecology* 105.3 (2024), e4244. ISSN: 1939-9170. DOI: 10.1002/ecy.4244.

[51] Anthony Sévêque et al. "Spatial Close-Kin Mark-Recapture Models Applied to Terrestrial Species with Continuous Natal Dispersal". In: *Methods in Ecology and Evolution* n/a.n/a (2024). ISSN: 2041-210X. DOI: 10.1111/2041-210X.14490.

[52] Chris C R Smith et al. "Dispersal Inference from Population Genetic Variation Using a Convolutional Neural Network". In: *Genetics* 224.2 (1st June 2023), iyad068. ISSN: 1943-2631. DOI: 10.1093/genetics/iyad068.

[53] Chris C. R. Smith and Andrew D. Kern. "disperseNN2: A Neural Network for Estimating Dispersal Distance from Georeferenced Polymorphism Data". In: *BMC Bioinformatics* 24.1 (11th Oct. 2023), p. 385. ISSN: 1471-2105. DOI: 10.1186/s12859-023-05522-7.

[54] Chris C. R. Smith et al. "Estimation of Spatial Demographic Maps from Polymorphism Data Using a Neural Network". In: *Molecular Ecology Resources* 24.7 (2024), e14005. ISSN: 1755-0998. DOI: 10.1111/1755-0998.14005.

[55] John D. Swenson et al. "Accounting for Unobserved Population Dynamics and Aging Error in Close-Kin Mark-Recapture Assessments". In: *Ecology and Evolution* 14.2 (2024), e10854. ISSN: 2045-7758. DOI: 10.1002/ece3.10854.

[56] Brian D. Taras et al. "Estimating Demographic Parameters for Bearded Seals, Erignathus Barbatus, in Alaska Using Close-Kin Mark-Recapture Methods". In: *Evolutionary Applications* 17.11 (2024), e70035. ISSN: 1752-4571. DOI: 10.1111/eva.70035.

[57] Alvaro Tejero-Cantero et al. "Sbi: A Toolkit for Simulation-Based Inference". In: *Journal of Open Source Software* 5.52 (2020), p. 2505. DOI: 10.21105/joss.02505.

[58] Verena M Trenkel et al. "Close-Kin Mark–Recapture Abundance Estimation: Practical Insights and Lessons Learned". In: *ICES Journal of Marine Science*

79.2 (10th Mar. 2022). Ed. by Lorenz Hauser, pp. 413–422. ISSN: 1054-3139, 1095-9289. DOI: 10.1093/icesjms/fsac002.

[59] Andrea K. Turkalo, Peter H. Wrege and George Wittemyer. "Demography of a Forest Elephant Population". In: *PLOS ONE* 13.2 (15th Feb. 2018). Ed. by Alfred L. Roca, e0192777. ISSN: 1932-6203. DOI: 10.1371/journal.pone.0192777.

[60] Robin S. Waples. "The Idiot's Guide to Effective Population Size". In: *Molecular Ecology* n/a.n/a (), e17670. ISSN: 1365-294X. DOI: 10.1111/mec.17670.

[61] Robin S. Waples and Pierre Feutry. "Close-Kin Methods to Estimate Census Size and Effective Population Size". In: *Fish and Fisheries* 23.2 (2022), pp. 273–293. ISSN: 1467-2979. DOI: 10.1111/faf.12615.

[62] George Wittemyer, David Daballen and Iain Douglas-Hamilton. "Comparative Demography of an At-Risk African Elephant Population". In: *PLOS ONE* 8.1 (16th Jan. 2013), e53726. ISSN: 1932-6203. DOI: 10.1371/journal.pone.0053726.

[63] K. D. Young, S. M. Ferreira and R. J. Van Aarde. "Elephant Spatial Use in Wet and Dry Savannas of Southern Africa". In: *Journal of Zoology* 278.3 (2009), pp. 189–205. ISSN: 1469-7998. DOI: 10.1111/j.1469-7998.2009.00568.x.